PRECAST LIGHTWEIGHT CONCRETE PANELS REINFORCED WITH GLASS FIBER REINFORCED POLYMER BARS

by

Brandon Tyler Besser

A thesis submitted to the faculty of
The University of Utah
in partial fulfillment of the requirements for the degree of

Master of Science

Department of Civil and Environmental Engineering

The University of Utah

May 2011

The University of Utah Graduate School

STATEMENT OF THESIS APPROVAL

The thesis of **Brandon Tyler Besser**

has been approved by the following supervisory committee members:

Chris P. Pantelides	, Chair	**11/9/2010** Date Approved
Lawrence D. Reaveley	, Member	**11/9/2010** Date Approved
Pedro Romero	, Member	**11/9/2010** Date Approved

and by **Paul J. Tikalsky** , Chair of

the Department of **Civil and Environmental Engineering**

and by Charles A. Wight, Dean of The Graduate School.

ABSTRACT

Corrosion of traditional steel reinforcement used in reinforced concrete bridges and parking structures exposed to water and deicing salts is of major concern. The chloride-induced corrosion of traditional steel reinforcement weakens the reinforced concrete member as well as adding to the annual maintenance cost of the structure. The resistance to corrosion of Glass Fiber Reinforced Polymer (GFRP) bars as reinforcement provides a viable alternative to steel reinforcement in areas where deterioration of steel reinforcement is an issue. Additional benefits can be obtained through the use of lightweight concrete. Lightweight concrete can allow structural members to be lighter, which is advantageous for lifting and moving operations when precast concrete elements are used. This thesis evaluates the one-way shear capacity of precast lightweight concrete panels reinforced with GFRP reinforcement. A total of six precast concrete specimens consisting of three normal weight concrete specimens and three lightweight concrete specimens reinforced with GFRP reinforcement were tested and compared. Finally, the results are compared to the theoretical shear predictions of the ACI 440.1R-06 and those provided by previous research conducted by Mr. Neil Hoult of the University of Cambridge, UK.

TABLE OF CONTENTS

LIST OF FIGURES

Figure Page

LIST OF TABLES

Tables Page

LIST OF SYMBOLS AND ABBREVIATIONS

GFRP	=	Glass Fiber Reinforced Polymer
ACI	=	American Concrete Institute
AASHTO	=	American Association of State and Highway Transportation Officials
LRFD	=	Load and Resistance Factor Design
MCFT	=	Modified Compression Field Theory
FRP	=	Fiber Reinforced Polymer
LVDT	=	Linear Variable Displacement Transducer
ASTM	=	American Society for Testing and Materials
$K_{Precracking}$	=	Precracking stiffness
$K_{Postcracking}$	=	Postcracking stiffness
I_g	=	Gross moment of inertia
$I_{uncracked}$	=	Uncracked moment of inertia
$I_{cracked}$	=	Cracked moment of inertia
V_c	=	Concrete shear resistance
V_s	=	Shear reinforcement resistance
f'_c	=	Concrete compressive strength
b_w	=	Specimen width
d	=	Depth from extreme compressive fiber to centroid of flexural reinforcement

k	=	Ratio of neutral axis depth to GFRP tendon depth
ρ_f	=	GFRP reinforcement ratio
A_f	=	Area of flexural reinforcement
n_f	=	Modular ratio
E_c	=	Modulus of elasticity of GFRP
E_f	=	Modulus of elasticity of concrete
λ	=	Strength reduction factor
ε_x	=	Longitudinal strain at middepth at predicted shear failure level
s_{xe}	=	Effective crack spacing and size effect
b_w	=	Web width
d_v	=	Effective shear depth
a_g	=	Maximum aggregate size
M_f	=	Bending moment at critical section for shear
V_f	=	Shear force at critical section for shear

ACKNOWLEDGEMENTS

The author would like to acknowledge the financial support of the Utah Department of Transportation as well as the Expanded Shale, Clay and Slate Institute. The author would also like to acknowledge the contribution of Hanson Eagle Precast for manufacturing the GFRP panels. The author would like to acknowledge the invaluable contributions and hard work of Ruifen Liu, whose efforts made this project possible. Additionally, he would like to acknowledge the assistance of Professor Chris Pantelides, Professor Lawrence D. Reaveley and Mark Bryant of the University of Utah.

CHAPTER 1

INTRODUCTION

1.1 Introduction

Deterioration of reinforcing steel in traditional reinforced concrete is of great concern in areas where chlorine-induced corrosion is an issue. Traditional reinforcing steel is protected from corrosion by the alkalinity of the surrounding concrete. However, when structures such as bridges and parking structures are exposed to deicing salts and water, the alkalinity of the concrete can be reduced, leading to corrosion of the steel reinforcement. The use of Fiber Reinforced Polymer reinforcing in the United States of America grew in popularity in the early 1980s as advanced technology, such as Magnetic Resonance Imaging, required concrete reinforcement that was electrically nonconductive. The use of Glass Fiber Reinforced Polymer (GFRP) reinforcing bars has increased considerably from the 1980s and is now a viable alternative to the use of traditional steel reinforcing in areas where corrosion is a problem or the reinforcement needs to be thermally or electrically nonconductive. The chemical composition of GFRP reinforcing makes it essentially immune to chlorine-induced deterioration. Additionally, the use of lightweight concrete panels can allow for a reduced superstructure weight, which is beneficial for lifting and moving operations when precast concrete elements are being used. An additional possible benefit of a lighter superstructure is a reduction in the size and weight of the substructure. However, currently, there is a lack of data for the

performance of precast lightweight concrete panels reinforced with GFRP reinforcing. The current ACI 440.4R-06[1] and the new AASHTO LRFD[2] document on GFRP bridge decks do not provide theoretical design equations for the use of lightweight concrete reinforced with GFRP reinforcing bars. Additionally, the shear capacity predictions of Hoult[3], which are based on the theoretical model of the Modified Compression Field Theory (MCFT) have been evaluated to determine their applicability for the use of lightweight concrete reinforced with GFRP reinforcement. Tests have been conducted on both normal weight and lightweight concrete specimens reinforced with GFRP reinforcing to determine if the current shear capacity equations for normal weight concrete reinforced with GFRP reinforcement are adequate to predict the shear capacity when lightweight concrete is used.

1.2 Background

Expansive corrosion of the reinforcing steel of traditional reinforced concrete is a serious problem in areas where deicing salts are used on concrete driving and parking surfaces during winter months. The inevitable cracking of concrete surfaces allows the steel reinforcement to be exposed to water and deicing salts, which leads to corrosion. As the steel reinforcement corrodes, it expands, causing the surrounding concrete to spall, exposing more steel reinforcement and causing further deterioration of the concrete. The corrosion of the reinforcing steel and the spalling of the concrete cover weaken the concrete element which can lead to a premature and sudden failure. The deterioration of the concrete and the reinforcing steel in a concrete element increases the annual maintenance costs of the structure as well as the overall lifetime cost of the structure.

The use of GFRP reinforcement in reinforced concrete has several advantages over traditional steel reinforcement. One of the main advantages is that GFRP bars are virtually immune to chloride-induced corrosion that is associated with deicing salts and marine environments. The resistance of GFRP reinforcement to corrosion prevents the bar from weakening or expanding when exposed to water and deicing salts. Since the reinforcement will not corrode or expand, the amount of spalling of cover concrete will be minimal and will result in a lower annual maintenance cost and lifetime cost of the structure.

GFRP reinforcement is produced in standard steel reinforcement sizes but has approximately one and a half times the tensile capacity of traditional steel reinforcement. While GFRP bars have a higher tensile strength than the standard steel bars they have about one fourth the weight of steel which allows for faster assembly of concrete members while reducing labor and production cost.

There are, however, drawbacks to the physical properties of GFRP bars. The modulus of elasticity of GFRP reinforcement is roughly one fifth that of traditional steel reinforcement. The lower modulus of elasticity of GFRP bars requires that either the reinforcement ratio of the concrete member be increased or that the members have an increased thickness to reduce deflections under service load conditions. An additional drawback of GFRP reinforcement is that the stress-strain relation is linear to failure. This stress-strain behavior indicates that there is no yielding of the GFRP reinforcement during loading and that failure by rupturing of the GFRP reinforcement will be sudden with no warning of impending failure. Because of this undesirable failure, the preferred

failure mode of concrete reinforced with GFRP reinforcement is that of concrete crushing rather than rupture of the GFRP reinforcement.

The use of GFRP reinforcement as an alternative to traditional steel reinforcement is cost competitive in areas where chloride-induced corrosion is an issue. The immunity of GFRP to corrosion allows for reduced maintenance costs as well as elimination of the protective membrane placed on many precast concrete decks. Although the GFRP bars have a higher initial cost, the lower maintenance costs can result in a lower long-term cost when compared to that of traditional steel reinforcement.

The lightweight concrete used in this research is a sand-lightweight concrete mix that uses Utelite Lightweight aggregate. Utelite Lightweight aggregate is an expanded shale lightweight aggregate produced east of Salt Lake City, Utah. The raw shale is crushed then heated in a rotary kiln until it is red hot and nearly plastic. At this high temperature, the internal gases in the aggregate are heated, causing the aggregate to expand resulting in a lower density. Once the aggregate has cooled, it retains the higher volume and has a density of roughly half that of traditional normal weight aggregate[4]. For sand-lightweight concrete, the remaining ingredients, being cement, water and fine aggregate, are the same as those used for normal weight concrete.

Lightweight concrete allows for the production of concrete members that have a lower unit weight while maintaining a compressive strength that is of the same magnitude desired in normal weight concrete. Superstructure members made of lightweight concrete may weigh less, which would allow for the substructure to be lighter which has both economic and seismic benefits. Lighter substructures use less materials, which corresponds to lower material and labor costs associated with construction. The reduced

weight of both the superstructure and the substructure reduces the seismic weight of the overall structure, which in turn reduces the horizontal shear produced during a seismic event.

An additional benefit of members made of lightweight concrete is that they can be easier to lift and move when Accelerated Bridge Construction or precast structural elements are used.

Presently, the ACI 440.1R-06[1] provides design information on the use of GFRP reinforcement with normal weight concrete. However, design information for the use of lightweight concrete and GFRP reinforcement is not currently provided by the American Concrete Institute (ACI). The new AASHTO LRFD[2] document on GFRP bridge panels also does not provide information for the use of GFRP reinforcement with lightweight concrete panels.

Previous research[3] has shown that the use of the MCFT can reliably predict the shear capacity of normal weight concrete elements reinforced with GFRP reinforcement. The 15 nonlinear equations, which must be solved simultaneously, are not practical for design codes. A set of simplifying assumptions proposed by Bentz[5] allowed the MCFT to be reduced to two equations while still providing accurate estimates of the shear capacity of steel or GFRP-reinforced concrete elements. These simplifying assumptions have been used by Hoult to predict the shear capacity of concrete elements reinforced with Fiber Reinforced Polymer (FRP) reinforcement. The shear predictions proposed by Hoult have been found to be reliable for normal weight concrete specimens reinforced with either steel reinforcement or GFRP reinforcement. However, one of the main simplifying assumptions used to develop the Hoult shear equations is that the shear

strength of concrete members without stirrups is controlled by aggregate interlock. Since aggregate interlock is largely ignored when lightweight concrete is used, the accuracy of the Hoult shear equations must be verified for lightweight concrete members.

The present research evaluates the use of the unmodified shear equations of the ACI 440.1R-06 for the use of precast lightweight concrete panels reinforced with GFRP reinforcement. Additionally, the use of the simplified Modified Compression Field Theory equations proposed by Hoult for steel reinforced concrete members are evaluated for the use of precast lightweight concrete panels reinforced with GFRP reinforcement.

CHAPTER 2

EXPERIMENTAL DESIGN

2.1 Precast Concrete Panels

Six precast concrete panels have been tested to determine the performance of both normal weight concrete and lightweight concrete reinforced with GFRP reinforcement. Both the normal weight concrete and lightweight concrete specimens were designed according to the guidelines of ACI 440.1R-06 for normal weight concrete reinforced with GFRP reinforcement. Each specimen had a length of 12 feet and a width of 2 feet. The thickness of the six specimens was 9.25 inches. The seemingly large thickness of the specimens is necessary because of the low modulus of elasticity of the GFRP reinforcement and to prevent excess deflection and cracking under normal loading conditions.

All of the specimens were reinforced identically with GFRP reinforcement on both the top and bottom of the specimen. The reinforcing mats consist of six #5 GFRP bars spaced at 4 inches on center in the long direction of the slab. GFRP reinforcement in the short direction of the slab consists of twenty-four #5 GFRP bars spaced at 6 inches on center, as can be seen in Figure 1. Also, shown in Figure 1 is a cross section showing the thickness of the specimens as well as the clear cover of the top and bottom reinforcement. The longitudinal and transverse reinforcement bars were attached perpendicular to each other using a pneumatic air gun and plastic clips, shown in Figure 2 and Figure 3. No

shear reinforcement was used in any of the specimens. The GFRP reinforcement properties provided by the manufacturer are as follows: tensile strength = 95,000 psi, modulus of elasticity = 5,920,000 psi. The cover for the top mat was 1.75 inches and the bottom reinforcing cover was 1 inch.

The specimens were instrumented to gather data during testing. The top and bottom GFRP reinforcement had electronic strain gauges attached at key locations, as shown in Figure 4, to determine the strain in the reinforcement at different load levels. Additional electronic strain gauges were attached on the compressive face of the concrete specimens at the same location as the GFRP strain gauges, as shown in Figure 5. The additional concrete gauges were placed on the extreme compression fiber of the specimens to measure the strain in the concrete during loading as well as to calculate the curvature when used with the strain in the bottom GFRP reinforcement. Additionally, three Linear Variable Displacement Transducers (LVDT) were attached to the specimens to measure the deflection under loading at different points. One LVDT was placed at the center of the specimen to measure the maximum midspan deflection. The remaining two LVDTs were placed 2 feet apart, on each side of the center LVDT, to measure the deflection at the quarter points of the specimen. Placement of the LVDTs can be found in the Experimental Setup section of this thesis.

The normal weight and lightweight concrete specimens were cast in a similar manner. The bottom mat cover was obtained by placing the reinforcement mat on plastic risers of a set height. The mat was then fixed into position using nails hammered into the formwork to prevent the GFRP reinforcement mat from floating out of place. The top reinforcement cover was obtained by hanging the top reinforcement mat from plastic

risers attached to a spanning wood support, as shown in Figure 6. The concrete was then poured into the framework, vibrated and finished by personnel at Hanson Structural Precast.

The concrete used for the normal weight specimens used a 3/4 inch coarse aggregate where the lightweight concrete used an expanded shale coarse aggregate (1/2 inch to the #4 sieve) manufactured by the Utelite company of Utah. Both the normal weight and lightweight specimens were cast from several batches of concrete and as a result have varying compressive strengths. No attempt was made to create normal weight concrete and lightweight concrete specimens with the same compressive strengths.

2.2 Experimental Setup

The specimens were loaded at the center point through a 10 inch by 20 inch by 1/2 inch thick steel plate that simulates the load area of an AASHTO design truck, as shown in Figure 7. The load was applied by a 500,000 pound capacity hydraulic actuator. The specimens were supported on concrete blocks that were 20 inches wide by 24 inches high that simulate support prestressed concrete bridge girders. To prevent damage to the support blocks as well as to provide a simple support 2 inch thick by 6 inch wide, elastomeric bearing pads were placed between the support blocks and the specimens. The specimens were simply supported with a center to center spacing of 96 inches. Figure 8 shows the full experimental set up.

The load was applied through the hydraulic actuator using increasing haver sine waves, as shown in Figure 9. The method of loading approximates the concentrated load of a wheel as it travels across the slab, in the short direction, at a constant velocity.

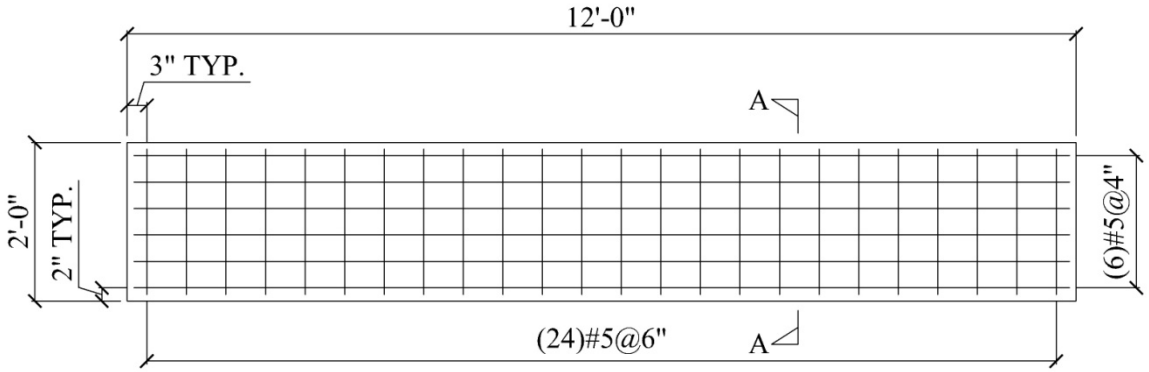

(a)

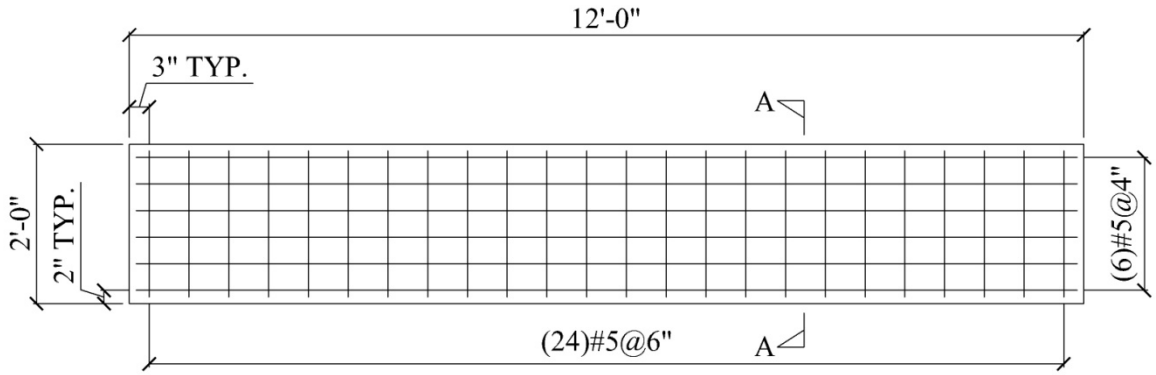

(b)

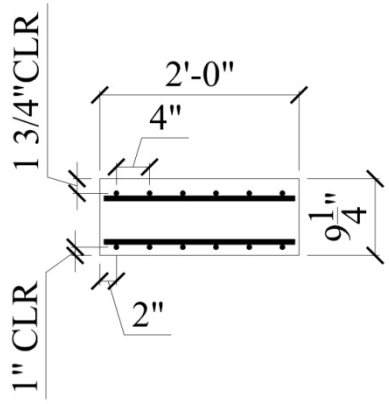

(c)

Figure 1 – Top and bottom GFRP reinforcement layout. (a) Top reinforcement. (b) Bottom reinforcement. (c) Section A-A

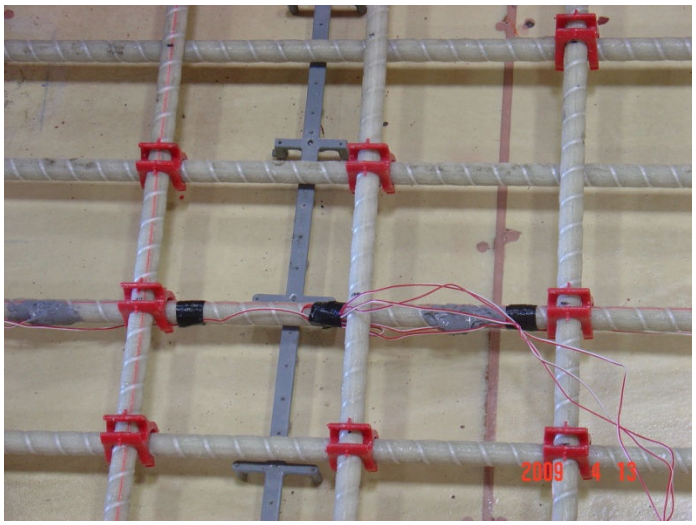

Figure 2 – Reinforcement mat attached with clip ties

Figure 3 – Kodi clip reinforcement ties

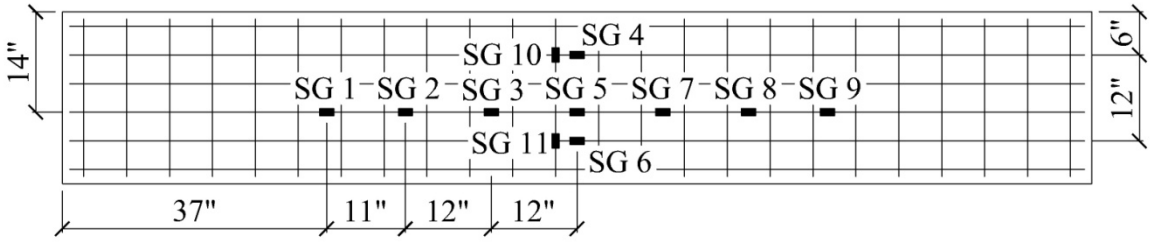

(a)

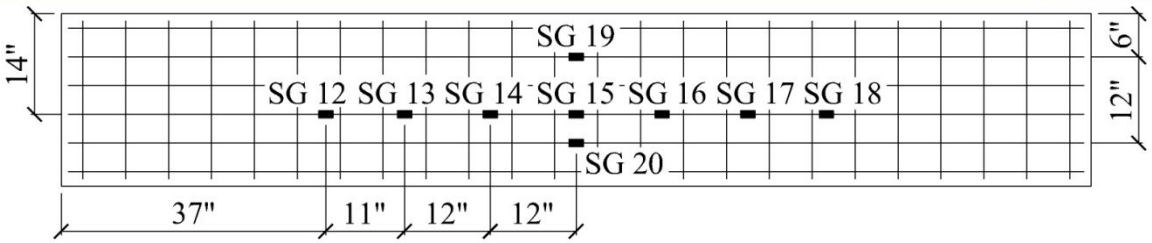

(b)

Figure 4 – Strain gauge placement. (a) Top mat. (b) Bottom mat.

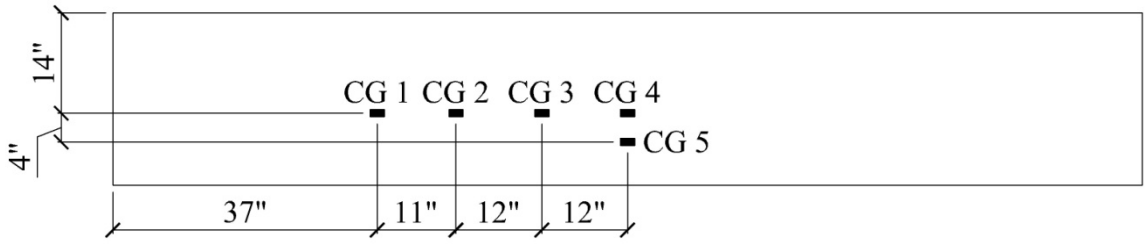

Figure 5 – Concrete strain gauge placement

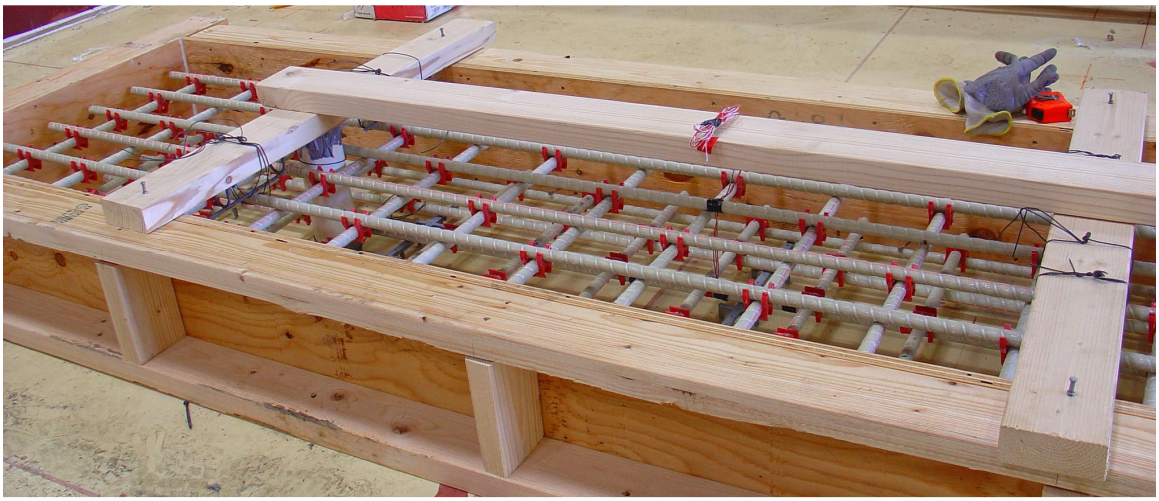

Figure 6 – Specimen formwork

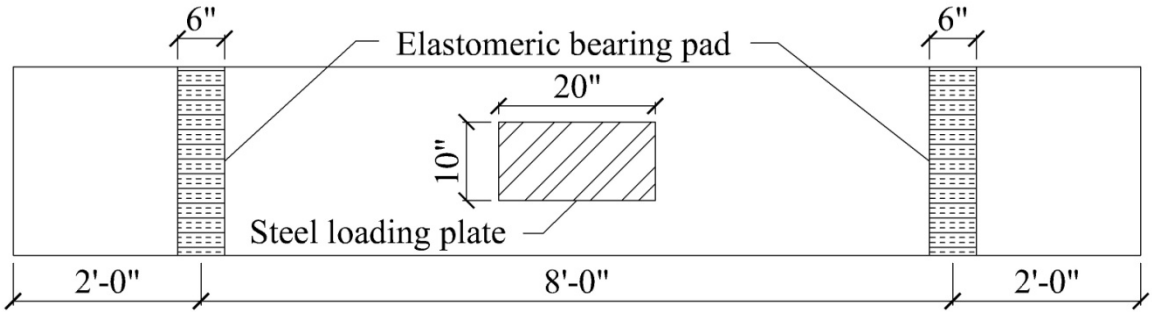

Figure 7 – Slab load application area and support points

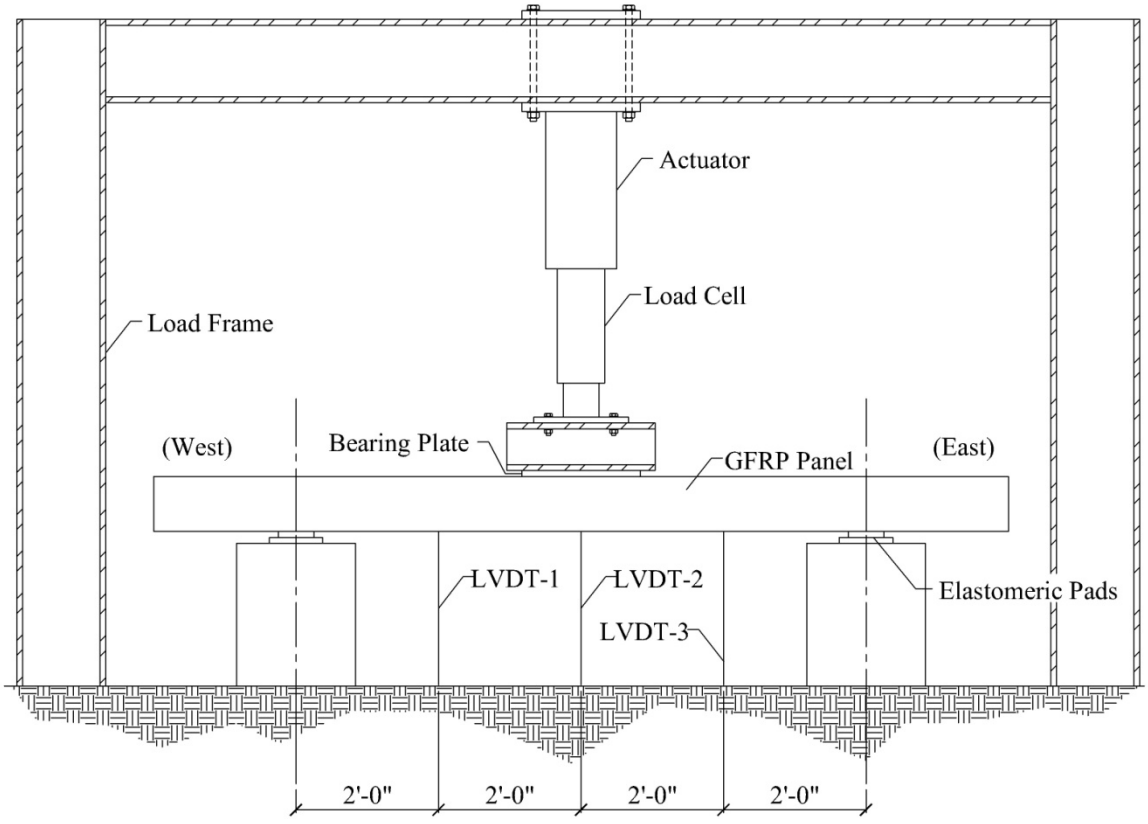

Figure 8 – Experimental setup

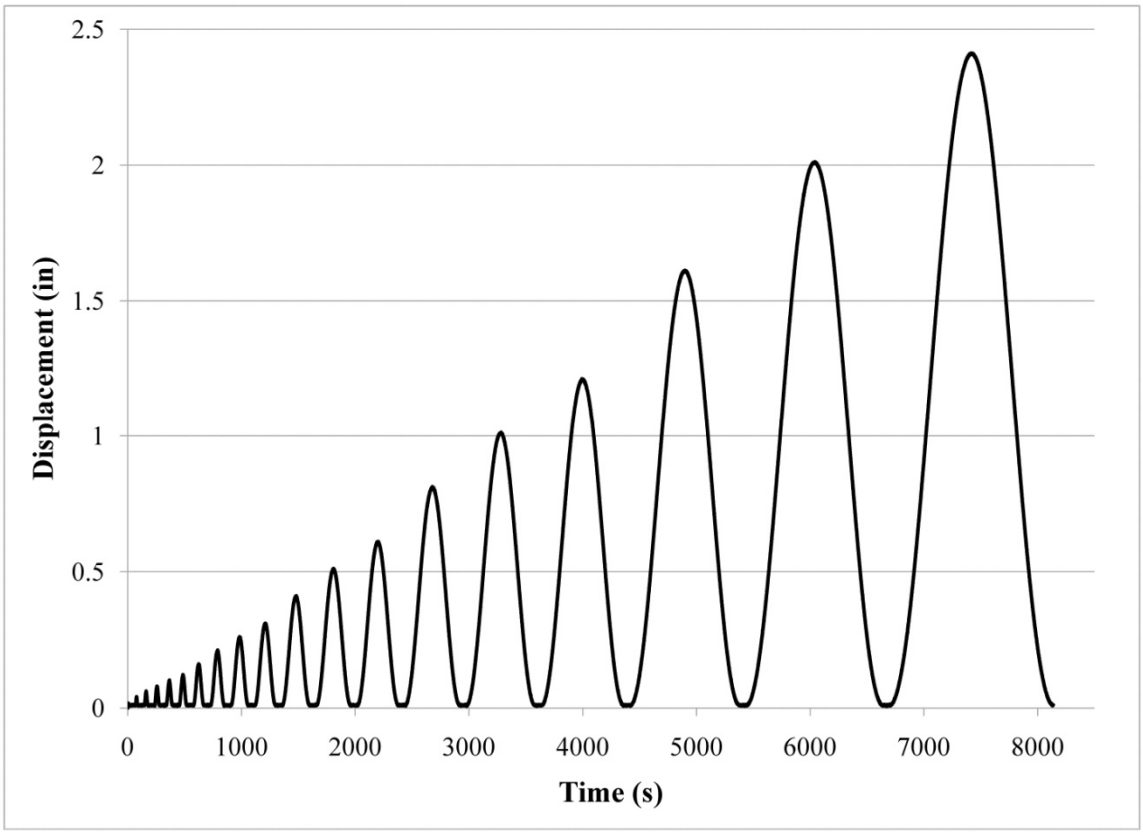

Figure 9 – Loading scheme

CHAPTER 3

RESULTS

3.1 Experimental Results

A summary of the experiments conducted on the six precast concrete panels consisting of three normal weight concrete specimens and three lightweight concrete specimens and reinforced identically with GFRP bars is given in Table 1. Table 1 includes the specimen designation, the concrete compressive strength at the day of testing, the maximum applied load at failure, the deflection at midspan at failure, maximum initial crack width prior to testing and the actual shear capacity of the precast concrete panels.

As shown in Table 1, some of the specimens have a value greater than zero for initial cracking of the slab. The initial cracking represents cracking of the specimens that was not a result of testing. There are several ways that the specimens may have become initially cracked prior to testing because of handling. The spacing between lifting points on the specimens may have been too wide, which would cause some cracking on the tension side of the specimens when they were lifted from the curing beds and loaded on the trailer to be transported to the University of Utah. Additional cracking occurred on some of the specimens as the result of the transportation trailer breaking during transportation, causing some of the specimens to fall off.

The compressive strength of the normal weight and lightweight concrete were measured by conducting compressive cylinder tests according to ASTM C873[6]. Three 4" diameter by 8" tall cylindrical samples were prepared for each specimen. The samples were crushed on the same day that the specimen was tested. The compressive strength shown in Table 1 is the average of the three compression tests. From Table 1 it can be seen that the compressive strength of the concrete used in this research is high strength concrete for both the normal weight concrete specimens and the lightweight concrete specimens. The concrete used consists of what was provided by the precast yard, and no effort was made to produce normal weight and lightweight concrete specimens with identical compressive strengths. The variation of the compressive strength of the specimens is a result of the specimens being cast from different concrete batches as well as being cast on different days. Additionally, the specimens were tested over a period of approximately 6 months, which allowed for different levels of hydration in the concrete and strengths greater than the 28-day strength.

According to Bridge Engineering[7] adaptation of the AASHTO Standard Specifications for Highway Bridges, the maximum expected traveling point load that would be applied to a bridge deck comes from a standard HS20-44 truck. The maximum single axle load applied by the HS20-44 truck is 32 kip. From Table 1 it can be seen that the HS20-44 truck does not provide a large enough point load on any of the specimens to cause a sudden failure of the specimen. With the HS20-44 truck having an axle spacing in the short direction of 6 feet and the clear spacing of the specimens being 8 feet, it is possible that both axles could load the specimens between the supports. However, the probability of this occurring in a standard bridge is unlikely.

During loading, the applied point load on the specimens increased according to the load scheme described earlier. As the load increased, the deflection increased accordingly. The deformation caused by high load levels can be seen in Figure 10.

Failure of all the specimens tested was due to a compressive shear failure with a large inclined crack and crushing of the concrete in the compressive zone. Failure of all specimens occurred on one side of the slab near the support and propagating diagonally to the applied load. Failure occurred on one side close to the left or right support, but never at both supports. The failure was sudden but not catastrophic. Additionally, no GFRP reinforcement ruptured during testing. Typical failure of the normal weight concrete specimens and typical failure of the lightweight concrete specimens is shown in Figure 11 and Figure 12, respectively. It is clear from Figure 11 and Figure 12 that failure mode of the normal weight concrete specimens and lightweight concrete specimens is essentially the same.

Three LVDTs used during testing were able to provide information on the displacement of the specimens at midspan as well as at the quarter points during loading. Two different service levels for the deflection of concrete members in building structures are given according to ACI 318-05[8] and are L/180 and L/480, where L is the clear span of the member in inches. The limit state of L/180 is meant for building structures where the immediate deflection is due to the application of temporary live loads and is given for flat roofs not supporting or attached to nonstructural elements likely to be damaged by large deflections. The limit state of L/480 is meant for building structures where the deflection is meant to be the sum of the long-term deflection due to all dead loads and immediate deflection due to additional live loads and is given from roof or floors that support or are

attached to nonstructural elements likely to be damaged by large deflections. An additional service level of L/800 for the deflection limit state of bridges without pedestrian walkways is given according to the AASHTO LRFD document, where L is the clear span of the member given in inches. Figure 13 shows the displacement of the specimens at the different service levels and at the ultimate condition. Specimens SP-4-LW and SP-5-LW are not included due to malfunctions of the testing equipment. It can be seen from Figure 13 that both the normal weight concrete specimens as well as the lightweight concrete specimens show largely symmetric levels of displacement throughout the testing. Symmetric levels of displacement indicate that the load applied to each side of the specimen was similar and that the cracking levels were similar on each side of the specimen. Additionally similar levels of displacement indicate that the stiffness is similar on each side of the specimen.

The midspan LVDT placed under the specimens during testing provided information that was used to create hysteretic load displacement figures, as seen in Figure 14. The hysteretic load-displacement curve for SP-4-LW is not available due to a malfunction of the hydraulic actuator described later.

The actual load-displacement figure for each specimen is able to be refined to a monotonic load-displacement envelope curve. The envelope load-displacement curve is created by determining the peak load and corresponding displacement of the specimen under each loading cycle and connecting the peak points with a straight line. Figure 15 shows the load-displacement envelope curves for the six specimens tested.

As can be seen in Figure 15 and Table 1, the normal weight concrete specimens are able to obtain a higher maximum load capacity and midspan displacement when

compared to the lightweight concrete specimens when the specimens are reinforced identically. When needed, the lower capacity and lower midspan deflection of the lightweight concrete specimens are properties that can be designed for by increasing the reinforcement ratio and the thickness of the member while still providing the advantages previously discussed.

By reducing the actual load-displacement curves to load-displacement envelope curves it can be observed that there is an obvious transition zone where the stiffness of the specimen is reduced. The transition zone defines where the specimen stiffness changed from the initial uncracked stiffness to the cracked stiffness, called precracking and postcracking, respectively. In the precracked region of the figure, there may be some minor cracking; however, this level of cracking is not sufficient to cause the drastic change in stiffness that can be observed at the transition zone between the precracked and postcracked stiffness levels.

The load-displacement envelope curves of Figure 15 can be further reduced to allow for the calculation of the actual precracking stiffness and postcracking stiffness of the specimens. By assuming that the variation in stiffness prior to cracking and after cracking is minimal, the load-displacement curves can be simplified to two linear segments, as seen in Figure 16. The first segment located in the lower left-hand section of each plot and denoted by $K_{Precracking}$ represents the precracking stiffness while the second segment denoted by $K_{Postcracking}$ represents the postcracking stiffness of the specimen. The precracking stiffness and postcracking stiffness of the normal weight concrete specimens and the lightweight concrete specimens is given in Figure 17.

The precracking stiffness is calculated by finding the slope of the precracking segment of each specimen in Figure 17. The postcracking stiffness is found by calculating the slope of the postcracking segment of each specimen in Figure 17. The calculated precracking stiffness and postcracking stiffness of the specimens are given in Table 2.

Table 2 shows that the precracking stiffness of the specimens has a large variation when it is compared within a single concrete type or when compared between the two different concretes types. The variation within the precracking stiffness of the specimens is a result of the different levels of cracking in the specimens, discussed previously. It can be seen that generally, the lightweight concrete specimens have a precracking stiffness that is lower than the precracking stiffness of the normal weight concrete specimens.

It should be noted that the precracking stiffness of specimen SP-4-LW is very low due to a malfunction with the hydraulic actuator during testing. At the start of the test, the actuator malfunctioned, causing the slab to be loaded rapidly and monotonically to failure. After failure, the unbroken portion of the specimen was shifted, allowing for the specimen to be retested. The clear span of the specimen remained 96 inches and a LVDT was able to be secured at the midspan of the specimen. However, the initial loading to failure of the specimen caused higher levels of cracking on the unbroken section of the specimen. Once the specimen was shifted, and the midspan LVDT was reattached, the specimen was reloaded to failure. The load and midspan displacement was recorded during reloading.

The postcracking stiffness of the six specimens shows a small level of variation. The average postcracking stiffness of the normal weight concrete specimens is approximately 10 % higher than that of the lightweight concrete specimens. The higher postcracking stiffness of the normal weight concrete is to be expected because of the higher concrete load capacity and deflection of the normal weight concrete specimens. The small variation in the postcracking stiffness between the normal weight concrete and lightweight concrete specimens indicates that the level of midspan displacement in relation to the postcracking load of the specimens is similar, and that at ultimate load, the difference in stiffness of the normal weight concrete specimens and the lightweight concrete specimens is minimal with a range of approximately 8 kip/in.

Ignoring specimens SP-4-LW and SP-5-LW, because of mechanical malfunction and cracking prior to testing described previously, it can be seen from Table 3 that the postcracking stiffness of both the normal weight concrete and lightweight concrete specimens range from 22 to 35 % of the precracking stiffness. It can also be seen that on average, the normal weight concrete specimens have a postcracking stiffness that is approximately 30% of the precracking stiffness of the normal weight concrete specimens. The lightweight concrete can be seen to have a postcracking stiffness that is approximately 25% of the precracking stiffness of the lightweight concrete specimen.

During loading, the strain in the bottom mat GFRP reinforcement as well as the strain in the concrete at the most extreme compressive fiber was measured and recorded using electronic strain gauges. The strain achieved in the GFRP reinforcement bars at the different service levels, discussed previously, at the ultimate condition and percent of

ultimate strain is given in Table 3. Table 4 gives the strain achieved in the concrete at the different service levels and at the ultimate condition.

It should be noted that a positive strain value indicates tension where a negative value indicates compression. Specimens with values of NA indicate that the information is not available. Information may not be available due to several reasons. SP-1-NW does not have concrete strain information because the concrete strain gauges were not decided upon until after the specimen was tested. In the case of specimen SP-3-NW, the concrete gauges were temporarily not activated during the initial cycles. SP-4-LW has no strain information due to the malfunction of the actuator during testing previously discussed.

Table 3 shows that difference in the levels of strain in the GFRP reinforcement obtained for both the normal weight concrete specimens and the lightweight concrete specimens during testing and at the ultimate condition is on average approximately 14% with neither concrete type showing consistently higher strain levels in the GFRP reinforcement. By using the manufacturer provided guaranteed tensile strength and modulus of elasticity, the maximum tensile strain of the GFRP reinforcement was found to be approximately 16,000 microstrains as compared to a maximum strain capacity of 2,000 microstrain for 60 ksi reinforcement steel. From Table 3 it becomes apparent that none of the GFRP reinforcing in either the normal weight concrete specimens or the lightweight concrete specimens reaches more than 76% of the ultimate tensile strain capacity of the GFRP reinforcement.

It can also be seen from Table 4 that the strain levels in concrete for the normal weight concrete specimens and the lightweight concrete specimens during testing and at the ultimate condition have a difference on average of approximately 11% with neither

concrete type showing consistently higher strain levels in the compression zone of the specimens. Both the normal weight concrete specimens as well as the lightweight concrete specimens reach an average compressive strain value in the concrete that is just under 70% of the ultimate recommended design concrete strain of 3,000 microstrain. This indicates that the use of lightweight concrete will result in strain levels that are predictable and able to be designed for while still enabling the benefits of lightweight concrete to be used.

Figure 18 shows the strain distribution in the bottom GFRP reinforcement over the length of the specimens. In Figure 18, the strain at each end of the slab is assumed to be zero. The strain in the GFRP reinforcement is assumed to increase or decrease linearly between points of known strain values.

It can be seen from Figure 18 that the strain levels in the bottom GFRP reinforcement are generally symmetric at low displacement levels. As the displacement becomes higher, the strain increases and the distribution across the length of the slab becomes less symmetric. The cause of the strain distribution figures becoming less symmetric as the loading increases is a result of increasing levels of cracking in the specimen. At high load levels, the cracking becomes less symmetric, causing the asymmetric strain distribution in the GFRP reinforcement.

Figure 19 shows the change in maximum crack width in the normal weight concrete specimens as well as the lightweight concrete specimens as the load level increases. Also shown in Figure 19 is the applied moment during testing. By knowing the moment level where cracking starts and at what load levels the cracking increases, it may be possible to estimate the applied moment on similar concrete elements by

measuring the width of cracks in the elements. Table 5 gives the maximum load during each load cycle, the maximum measured crack width once the load has been removed, the number of cracks observed after loading and the average crack spacing after loading. Information for SP-4-LW is again omitted from Figure 19 and Table 5 due to the malfunction of the testing equipment as described earlier.

Figure 19 shows that the maximum width of the cracks found in both the normal weight concrete specimens and the lightweight concrete specimens are of a similar magnitude when the load level is similar. The maximum crack width of the normal weight concrete specimens at the ultimate condition is greater than that of the lightweight concrete specimens. The larger crack widths of the normal weight concrete specimens is to be expected since the normal weight concrete specimens are able to sustain a higher maximum load level as well as a higher maximum deflection prior to failure.

From Table 5 it can be seen that the load level where cracking is initiated varies from specimen to specimen. However, once cracking has been initiated, the load level where the crack width begins to increase is similar in all specimens and occurs at roughly 12 kips. It can also be seen that the final number of cracks observed as well as the final average crack spacing is very similar for both the normal weight concrete specimens and the lightweight concrete specimens. The final number of cracks for all specimens has a range of 20 to 23 cracks with an average crack spacing ranging from 3.10 inches to 3.24 inches. Although the load level, number of cracks and crack spacing is different for each specimen at the initiation of cracking, the final cracking level due to the increase in loading reaches approximately the same level regardless of the use of normal weight concrete or lightweight concrete.

Figure 20 shows the moment-curvature relationship for the normal weight concrete specimens as well as the lightweight concrete specimens. Due to previously described equipment malfunctions, SP-4-LW is not included. Due to equipment malfunction, the lower moment-curvature values of SP-3-NW are not available, and have been assumed to be linear from the origin to the first known point, as shown with a dot-dash line.

From Figure 20 it can be seen that once initial cracking occurs just after a moment of 200 kip-inches, all the specimens have a relatively linearly increasing moment-curvature slope. For all specimens, the maximum measured strain value at the end of each loading cycle was used to calculate curvature. The nonlinearity of specimens SP-1-NW and SP-5-LW is due to the way in which the curvature of the specimens was calculated. For these two specimens, the measured strain values of the top and bottom mat GFRP reinforcement was used to calculate the curvature of the specimens. The more drastic changes in the slope of the moment curvature relation for SP-1-NW and SP-5-LW at higher curvature and moment levels was caused by the neutral axis moving from below the top mat reinforcement to above the top mat reinforcement as the load levels increased. The curvature of these two specimens was calculated in such a manner due to the unavailability of extreme compressive concrete strain values. All other specimens used the measured strain in the bottom GFRP reinforcing and the strain in the concrete at the extreme compressive fiber to calculate the curvature of the specimen. The slope of the moment-curvature relationship is equal to the modulus of elasticity of the concrete times the effective moment of inertia of the specimens. It can be seen that the slope of the moment-curvature relationship is different for each of the six specimens. The

difference in the slope of the moment-curvature relationship between the different specimens is a result of several factors. Higher compressive strengths of concrete result in higher values for the modulus of elasticity of the concrete, which can increase the slope of the moment-curvature relation. Another factor resulting in the difference in slope of the moment-curvature relationship is the extent of cracking in the specimen. As the specimen becomes cracked under loading, the moment of inertia of the specimen that is able to resist the applied load and bending is reduced. As the level of loading and level of cracking increases, the moment of inertia decreases.

Table 6 gives the gross moment of inertia, the uncracked moment of inertia, the cracked moment of inertia, denoted as I_g, $I_{uncracked}$ and $I_{cracked}$, respectively. Additionally, the ratio of the uncracked moment of inertia to the gross moment of inertia as well as the ratio of the cracked moment of inertia to the gross moment of inertia is given for one normal weight concrete specimen and one lightweight concrete specimen.

Specimens SP-1-NW and SP-6-LW were chosen because of their similarities in the precracking and postcracking stiffness. The gross moment of inertia was calculated using the design dimensions of the specimens. The uncracked and cracked moment of inertia was calculated by dividing the applied moment by the modulus of elasticity of the concrete multiplied by the average curvature at the center of the specimen and the quarter point of the specimen. The uncracked moment of inertia is given as the point where the stiffness changes from the precracking stiffness to the postcracking stiffness. The cracked moment of inertia is given at the ultimate condition at the end of the post-cracking segment.

From Table 6 it can be seen that the uncracked and cracked moment of inertia of the lightweight concrete specimen is greater than that of the normal weight concrete specimen. The lightweight concrete specimen has an uncracked moment of inertia that is approximately 30% greater than the normal weight concrete specimen. The cracked moment of inertia of the lightweight concrete specimen is approximately 24% greater than the normal weight concrete specimen.

The lower uncracked and cracked moment of inertia of the normal weight concrete specimen is a result of the higher concrete modulus of elasticity of the normal weight concrete as well as the higher curvature values obtained by the normal weight concrete specimen.

As expected, neither the normal weight concrete specimens nor the lightweight concrete specimens showed any indication of yielding of the GFRP reinforcement prior to shear failure. It can also be observed from Figure 20 that the use of normal weight concrete does appear to be able to obtain higher levels of moment capacity, but does not appear to always obtain higher levels of curvature when compared to the lightweight concrete specimens, when the specimen thickness and reinforcement ratio is the same. The lower levels of obtainable moment capacity of the lightweight concrete specimens can be designed for by increasing the amount of reinforcement, increasing the depth of the member or both.

3.2 Theoretical Predictions

Six precast concrete slabs reinforced with GFRP reinforcement were tested to determine if the shear capacity predictions given by ACI 440.1R-06[1] and the shear

prediction from Hoult[3] for normal weight concrete are adequate for the use of lightweight concrete. A summary of the experimental results as well as the predicted shear capacity of the specimens is given in Table 7. Table 7 gives the specimen designation, compressive strength of the concrete on the day of testing, maximum applied load, actual shear capacity, ACI predicted shear capacity, first-order Hoult predicted shear capacity and the second-order Hoult predicted shear capacity, to be discussed shortly.

The design of GFRP-reinforced normal weight concrete members is governed by ACI 440.1R-06. The shear strength of GFRP-reinforced normal weight concrete members determined by ACI 318-05 is given as the sum of the shear resistance provided by the concrete V_C and the steel shear reinforcement V_S. Presently, the ACI 440.1R-06 does not provide theoretical design equation for the capacity of lightweight concrete reinforced with GFRP reinforcement. All six specimens were reinforced with identical top and bottom transverse and longitudinal GFRP reinforcement but did not have any shear reinforcing. The resulting ACI predicted shear capacity of the specimens is provided by the concrete shear resistance, V_C, only. The shear capacity of the concrete is given by

$$V_C = \left(\frac{5}{2}k\right) 2\sqrt{f_c'} b_w d \qquad (1)$$

where V_C is the shear resistance provided by the concrete, f'_C is the concrete compressive strength measured on the day of testing, b_w is the width of the specimen and d is the depth from the extreme compressive fiber of the specimen to the centroid of the flexural reinforcing.

$$k = \sqrt{2\rho_f n_f + (\rho_f n_f)^2} - \rho_f n_f \quad (2)$$

$$\rho_f = A_f / b_w d \quad (3)$$

$$n_f = E_f / E_c \quad (4)$$

where k is the ratio of neutral axis depth to GFRP tendon depth, ρ_f is the GFRP reinforcement ratio, A_f is the area of flexural GFRP reinforcement, n_f is the modular ratio and E_f and E_c are the modulus of elasticity of the GFRP reinforcement and the concrete, respectively.

From Table 7 it can be seen that the actual shear capacity is greater for the normal weight concrete specimens when compared to the lightweight concrete specimens. The higher normal weight concrete shear capacity is as expected due to the normal weight concrete being able to sustain a higher axial load prior to failure.

Equation 1 was used to predict the shear capacity of both the normal weight concrete specimens and the lightweight concrete specimens. From Table 7 it can be seen that the ACI shear prediction provides results that are conservative for both the normal weight concrete and lightweight concrete specimens. The ACI shear prediction for the lightweight concrete specimens provides a higher predicted shear capacity than that of the normal weight concrete specimens. The higher predicted shear capacity of the lightweight concrete specimens is a result of the lower unit weight of the lightweight concrete. Lower unit weight concrete results in a lower concrete modulus of elasticity, E_c, which in turn causes the value of the modular ratio, n_f, to increase. A larger value of

the modular ratio provides a larger k value, which in turn provides a larger prediction of the shear capacity of the lightweight concrete specimens.

Table 8 gives a comparison of the actual shear capacity of the normal weight concrete specimens and the lightweight concrete specimens to the shear capacity predicted by using the ACI shear prediction of Equation 1.

Table 8 shows that the actual shear capacity of the normal weight concrete specimens is approximately 2.0 times the ACI predicted shear capacity for normal weight concrete reinforced with GFRP reinforcement. The actual capacity of the lightweight concrete specimens is approximately 1.5 times that found by applying Equation 1 for normal weight concrete reinforced with GFRP reinforcement to lightweight concrete specimens reinforced with GFRP reinforcement. While the shear predictions of Equation 1 provide conservative estimates for normal weight concrete and lightweight concrete reinforced with GFRP reinforcement, it can be seen that the factor of safety is greater for normal weight concrete reinforced with GFRP reinforcement.

In order to provide a higher factor of safety against failure for the lightweight concrete specimens, a modification factor can be applied to the ACI shear prediction given by Equation 1 for normal weight concrete reinforced with GFRP reinforcement. The standard strength reduction factor for sand-lightweight concrete is given as λ by the AASHTO LRFD[2] document and is given as 0.85. Equation 5 gives the ACI shear capacity prediction of Equation 1 modified for sand-lightweight concrete reinforced with GFRP reinforcement.

$$V_C = \left(\frac{5}{2}k\right)\lambda 2\sqrt{f_c'}b_w d \qquad (5)$$

$$\lambda = 0.85 \text{ for sand-lightweight concrete} \quad (6)$$

$$\lambda = 1 \text{ for normal weight concrete} \quad (7)$$

Table 9 gives the modified ACI shear capacity prediction of Equation 5, the actual shear capacity of the specimens and a comparison of the actual shear capacity to the modified ACI shear capacity prediction of Equation 5.

Table 9 shows that the modified ACI shear capacity predictions of Equation 5 for normal weight concrete reinforced with GFRP reinforcement remain the same with a margin of safety of approximately 2.0. It can be seen that by using the modified shear capacity prediction of Equation 5 for sand-lightweight concrete reinforced with GFRP reinforcement, the margin of safety is raised from approximately 1.5 to approximately 1.8.

In order to increase the safety margin of sand-lightweight concrete reinforced with GFRP reinforcement, a reduced strength reduction factor may need to be applied to the ACI shear capacity prediction of Equation 5. Table 10 shows how the use of a strength reduction factor 0.75 can increase the margin of safety for sand-lightweight concrete reinforced with GFRP reinforcing.

From Table 10 it can be seen that reducing the strength reduction factor in Equation 5 from 0.85 to 0.75 increases the margin of safety for sand-lightweight concrete reinforced with GFRP reinforcement from approximately 1.8 to 2.0. However, due to the limited number of tests performed, it is recommended that further research be conducted on additional specimens of varying size and reinforcement ratios prior to establishing the strength reduction factor as 0.75.

Table 7 indicates that the shear capacity predicted by the first-order simplified equation formulated by Hoult provides a predicted shear capacity that is even more conservative than the ACI shear prediction of Equation 1. The predicted shear capacity of the Hoult equation is given in MPa and mm units as

$$V_C = \frac{0.40}{(1+1500\varepsilon_x)} \times \frac{1300}{(1000+s_{xe})} \sqrt{f_c'} \times b_w d_v \qquad (8)$$

where ε_x is the longitudinal strain at middepth at the predicted shear failure level, s_{xe} is the effective crack spacing also known as the size effect, f'_c is the concrete strength, b_w is the web width and d_v is the effective shear depth, which is to be taken as 0.9d. The term s_{xe} in Equation 8 is the size effect term and is taken to be

$$s_{xe} = \frac{31.5d}{16+a_g} \geq 0.77d \qquad (9)$$

where a_g is the maximum aggregate size, in mm. It has been determined that in high strength concrete and lightweight concrete, the cracks tend to pass through the aggregate, rather than around it. Since the cracks pass through the aggregate, the aggregate size term in Equation 9 should be taken as zero for high strength concrete and lightweight concrete. The inclusion of the aggregate size term in Equation 9 allows the size effect term to be used for both normal weight concrete and lightweight concrete. Additionally, Equation 9 can be used for lightweight concrete without the use of a strength reduction factor for lightweight concrete. For the Hoult first-order and second-order shear predictions, an aggregate size of 3/4 inch was used.

Equation 8 includes a strain effect in the term ε_x. For concrete elements which are not subjected to axial loading and are not prestressed, Hoult[3] gives the strain as

$$\varepsilon_x = \frac{M_f/d_v + V_f}{2E_f A_f} \tag{10}$$

where M_f and V_f are the bending moment and shear force at the critical section for shear, respectively. E_f and A_f are as defined previously in Equation 3 and Equation 4.

For this research, an iterative approach is employed using a spreadsheet. This is done by estimating the longitudinal strain, ε_x, then evaluating Equation 8 to determine the shear strength at that strain level. Equation 10 is then evaluated to determine if the estimated strain is appropriate. By using the goal seek function in Microsoft Excel, a convergence of the estimated strain and the calculated strain is easily obtained. The spreadsheet employed was checked and refined using the example by Hoult[3] and was found to obtain the results given by the example. The values entered into the spreadsheet were in English units, which were then converted to SI units in order to use the Hoult first-order and second-order shear prediction equations.

Table 11 gives the actual shear capacity of the specimens as well as the Hoult first-order predicted shear found using Equation 8 and the ratio of the actual shear capacity to the Hoult first-order shear capacity.

From Table 11 it can be seen that for the six specimens tested, the Hoult first-order shear capacity predictions are overly conservative and provide a margin of safety of approximately 2.8 and 2.6 for the normal weight concrete specimens reinforced with

GFRP reinforcement and the lightweight concrete specimens reinforced with GFRP reinforcement, respectively.

Table 12 gives the actual maximum strain obtained in the longitudinal reinforcing, the Hoult predicted maximum strain, and the ratio of the maximum actual strain obtained to the Hoult predicted maximum strain and the Hoult predicted percent of the ultimate strain.

Table 12 shows that the Hoult predicted strain in the longitudinal reinforcement is very conservative. The actual strain in the GFRP reinforcement at failure of the specimens is approximately 2.0 times as much as the Hoult first-order predicted longitudinal strain. It can also be seen that the maximum Hoult predicted strain in the longitudinal reinforcing is at most 39% of the ultimate manufacturer specified maximum strain. In order to take advantage of the strain levels that are able to be obtained by the longitudinal reinforcing, a factor that increases the strain term in Equation 10 may be implemented for the first-order shear prediction. The implementation of a factor to increase the strain term in Equation 10 would result in a higher predicted shear capacity for the Hoult first-order prediction of Equation 8. A higher predicted shear capacity would make the predicted capacity be less overly conservative and allow for the more efficient use of materials. Additional research needs to be conducted on more specimens of varying size and reinforcement ratio to determine what the strain modification factor for Equation 10 should be.

Equation 8 is proposed by Hoult for steel reinforced concrete members where the strain in the longitudinal reinforcing is seldom greater than 1000 microstrain. When GFRP reinforcement is used, the strain in the longitudinal reinforcement is able to obtain

higher strain values. To account for the higher obtainable strain in the GFRP reinforcement, a second-order equation has been formulated by Hoult[3]. The second-order equation which produces more accurate estimates of the shear strength of a concrete member reinforced with GFRP reinforcement is given as

$$V_C = \frac{0.30}{0.5+(1000\varepsilon_x+0.15)^{0.7}} \times \frac{1300}{(1000+s_{ze})}\sqrt{f_c'} \times b_w d_v \qquad (11)$$

Equation 11 is able to be directly substituted for Equation 8 to provide a less conservative estimate of shear capacity for concrete specimens reinforced with GFRP reinforcement.

Table 13 gives the actual shear capacity of the specimens as well as the Hoult second-order predicted shear found using Equation 11 and the ratio of the actual shear capacity to the Hoult second-order shear capacity.

From Table 13 it can be seen that the Hoult second-order shear capacity prediction of Equation 11 provides a much more reasonable prediction of the shear capacity of concrete members reinforced with GFRP reinforcement. The margin of safety for the Hoult second-order shear capacity prediction was approximately 2.0 and 1.8 for the normal weight concrete specimens reinforced with GFRP reinforcement and lightweight concrete specimens reinforced with GFRP reinforcement, respectively.

Table 14 gives the actual maximum strain obtained in the longitudinal reinforcing, the Hoult second-order predicted maximum strain, and the ratio of the maximum actual strain obtained to the Hoult second-order predicted maximum strain and the Hoult percent of the ultimate strain.

From Table 14 it can be seen that the use of the Hoult second-order shear capacity prediction of Equation 11 allows higher longitudinal strain to be used when predicting the

shear capacity of the concrete specimens. Equation 11 uses a maximum strain that is 58% and 49% of the ultimate maximum strain obtainable in the GFRP reinforcement for normal weight concrete specimens and lightweight concrete specimens, respectively.

It can be seen that the Hoult second-order shear capacity prediction is less conservative for lightweight concrete members reinforced with GFRP reinforcement. However, the difference between the predicted shear capacity of the normal weight concrete specimens and the lightweight concrete specimens is approximately 10%, which corresponds to the modified ACI shear prediction, indicating that a strength reduction factor for the use of lightweight concrete may be unnecessary when the Hoult second-order equation is used. Additional research using the Hoult second-order shear prediction and lightweight concrete members of varying size and reinforcement ratios should be conducted to verify that a strength reduction factor is not needed for lightweight concrete members reinforced with GFRP reinforcement.

Table 1 – Summary of results

Designation	f'c (psi)	Max Load (kip)	Midspan Deflection (in)	Max Initial Crack Width (in)	Shear Capacity (kip)
SP-1-NW	8760	53.38	1.63	0.000	26.69
SP-2-NW	10370	59.37	1.85	0.002	29.69
SP-3-NW	12650	58.65	1.59	0.000	29.33
SP-4-LW	9090	48.66	1.49	0.002	24.33
SP-5-LW	8700	44.50	1.51	0.000	22.25
SP-6-LW	10930	44.32	1.51	0.002	22.16

Note - NW = Normal weight concrete
LW = Lightweight concrete

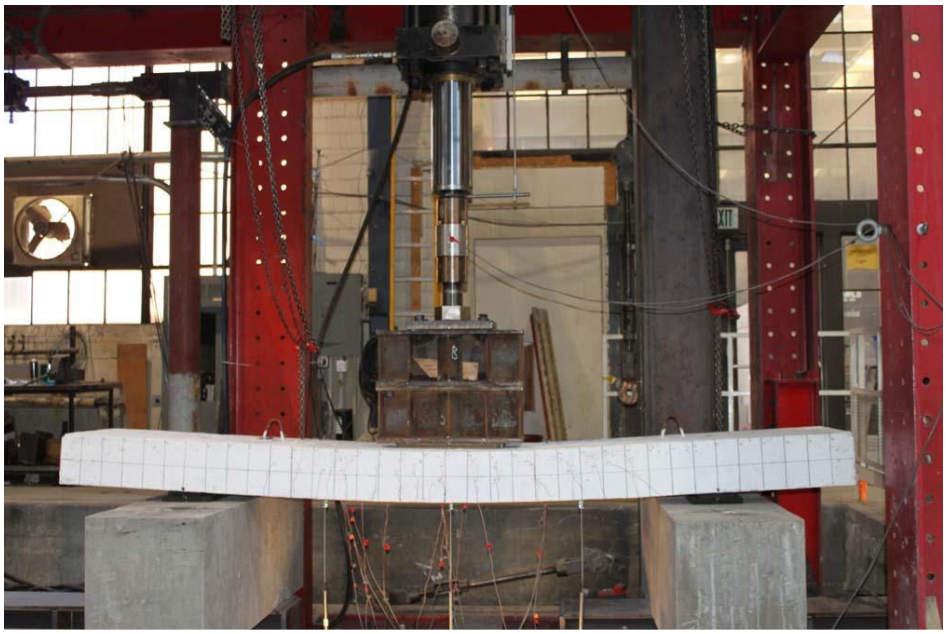

Figure 10 – Deformed shape

Figure 11 – Typical normal weight concrete specimen failure

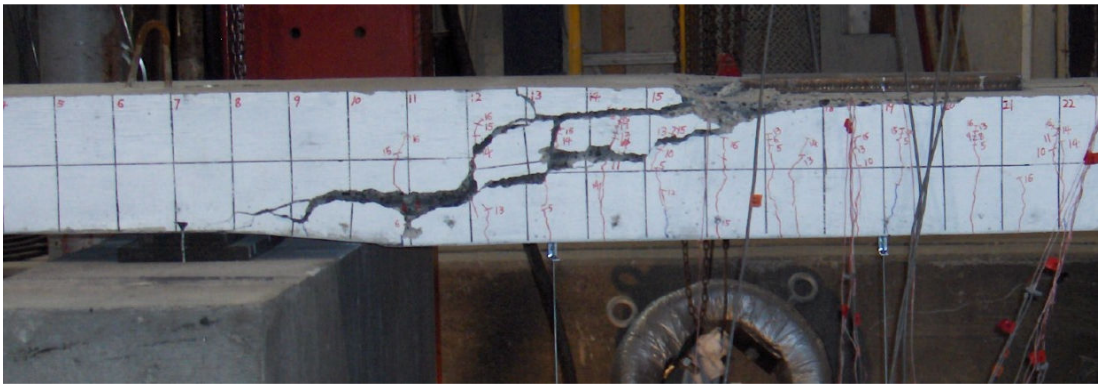

Figure 12 – Typical lightweight concrete specimen failure

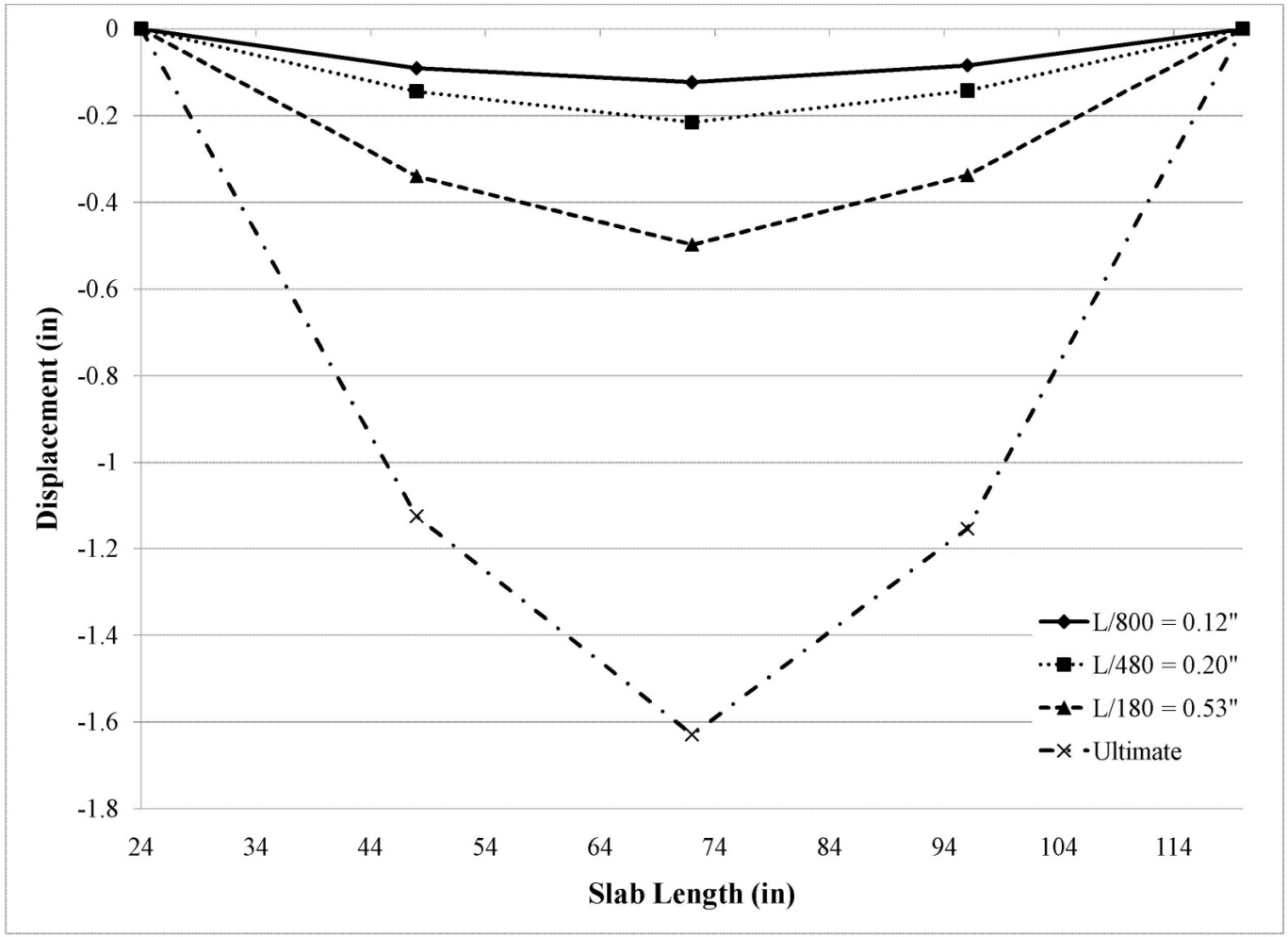

(a)

Figure 13 – Displacement of specimens at midspan and quarter points: (a) SP-1-NW displacement, (b) SP-2-NW displacement, (c) SP-3-NW displacement, (d) SP-6-LW displacement

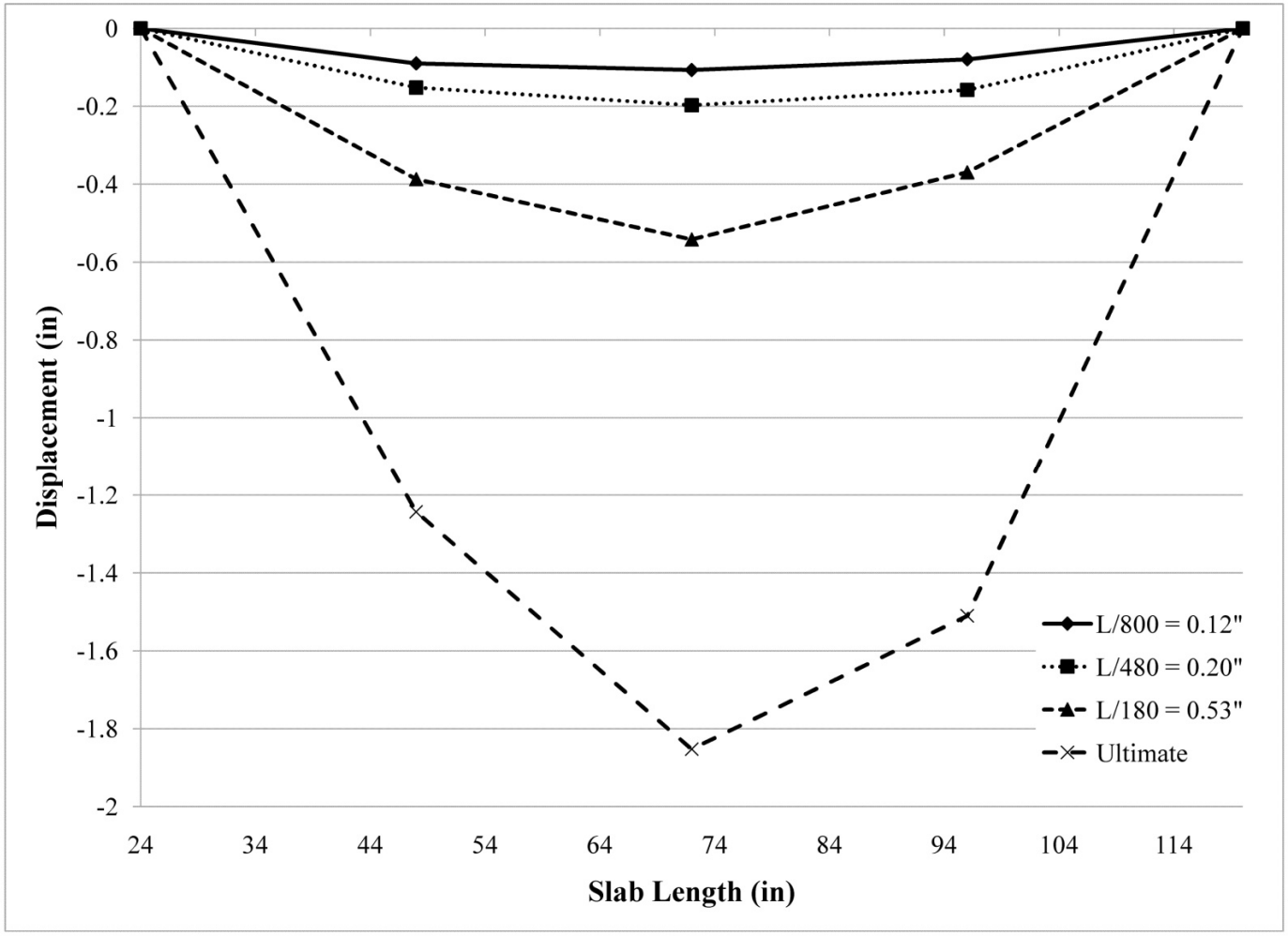

(b)
Figure 13 continued

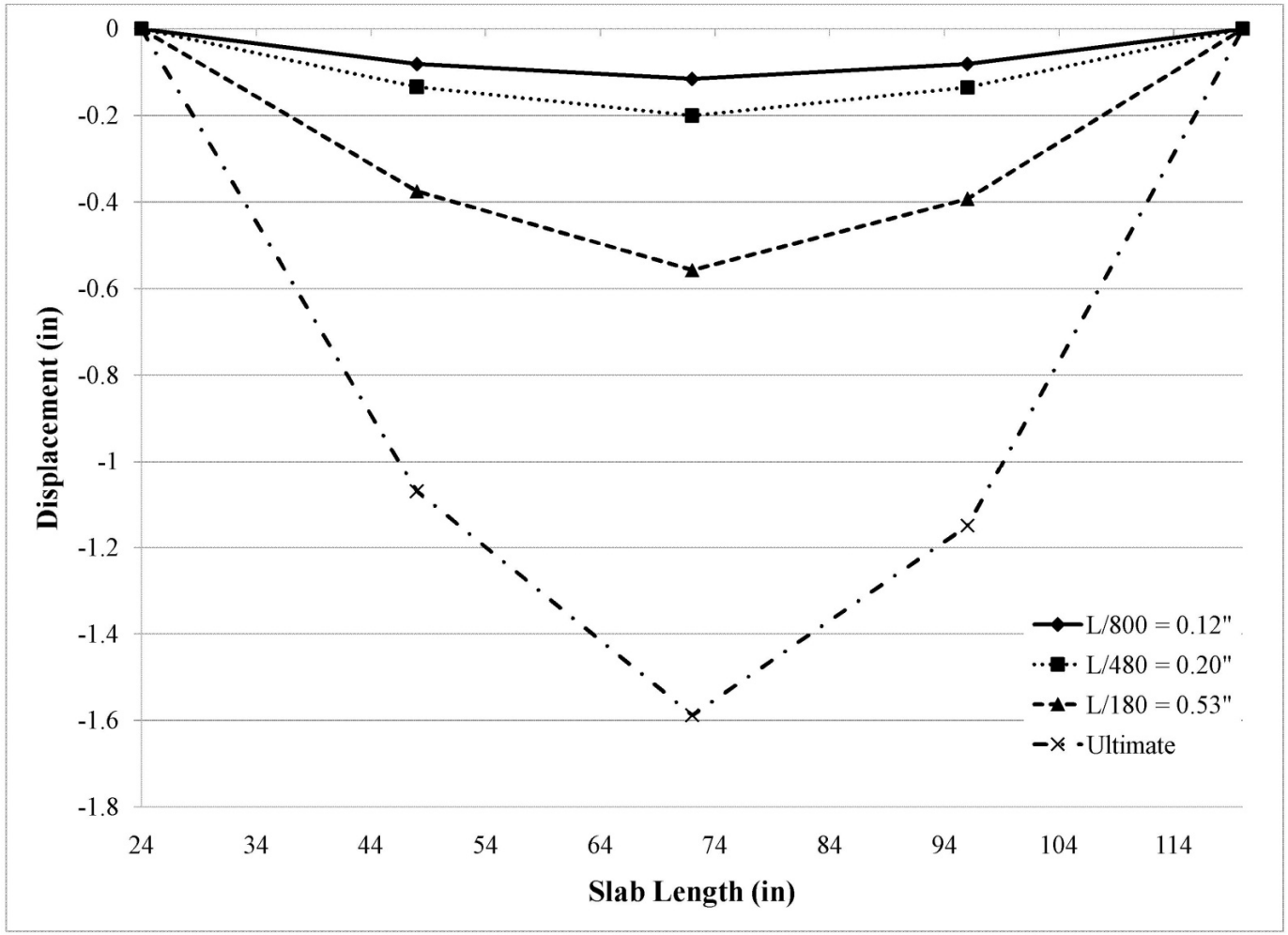

(c)

Figure 13 continued

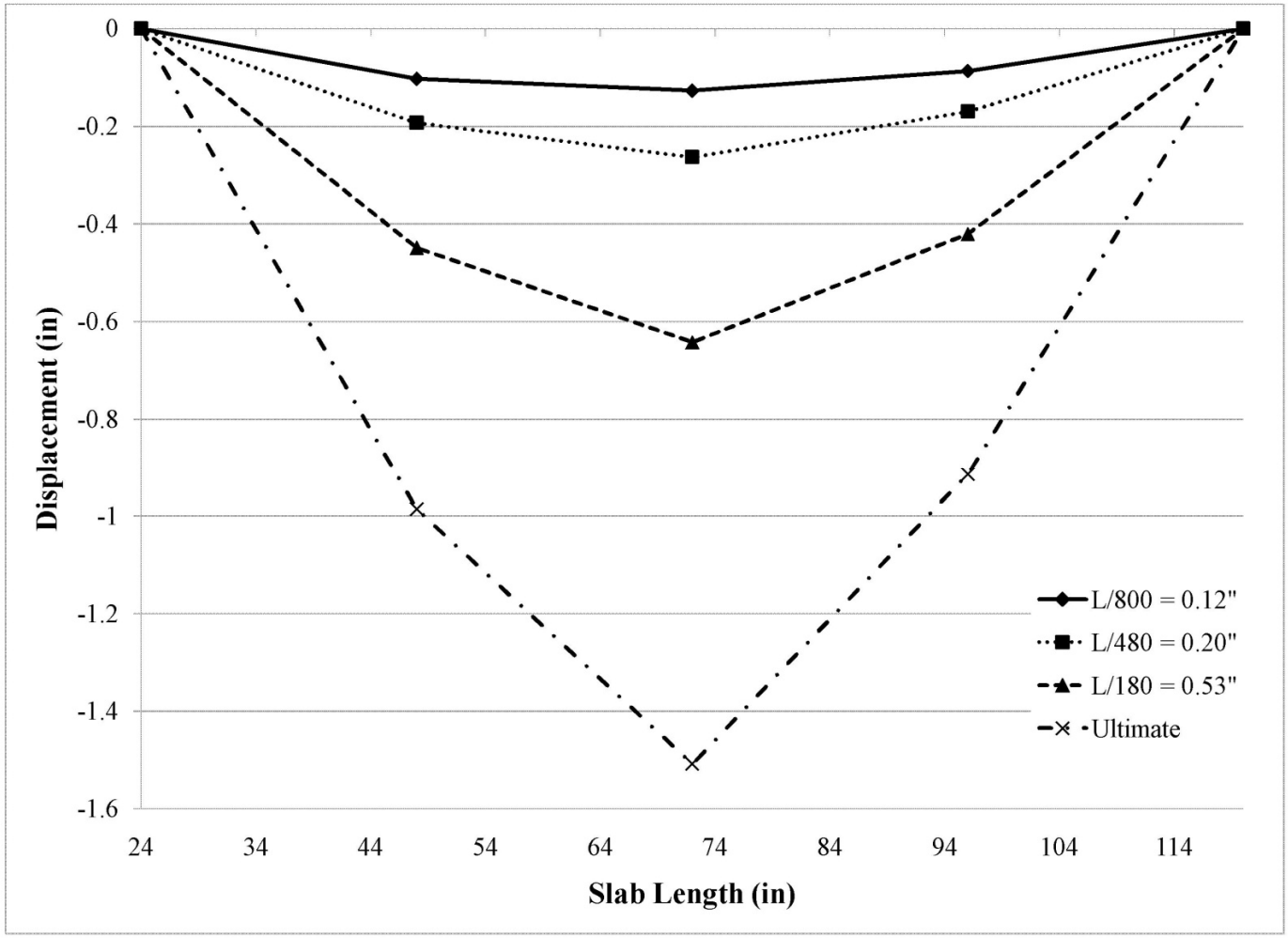

(d)

Figure 13 continued

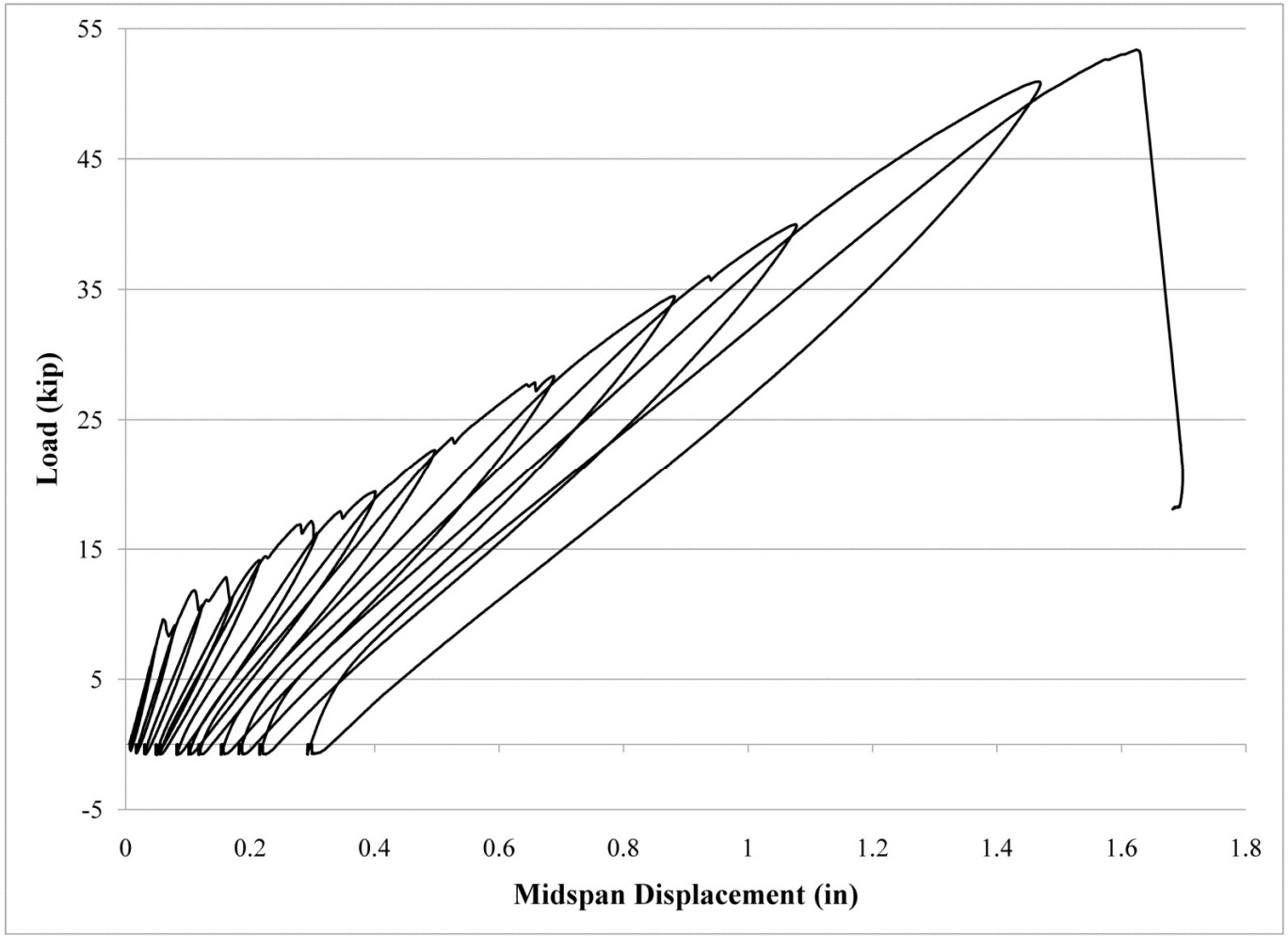

(a)

Figure 14 – Hysteretic load-displacement of specimens: (a) SP-1-NW, (b) SP-2-NW, (c) SP-3-NW, (d) SP-5-LW, (e) SP-6-LW

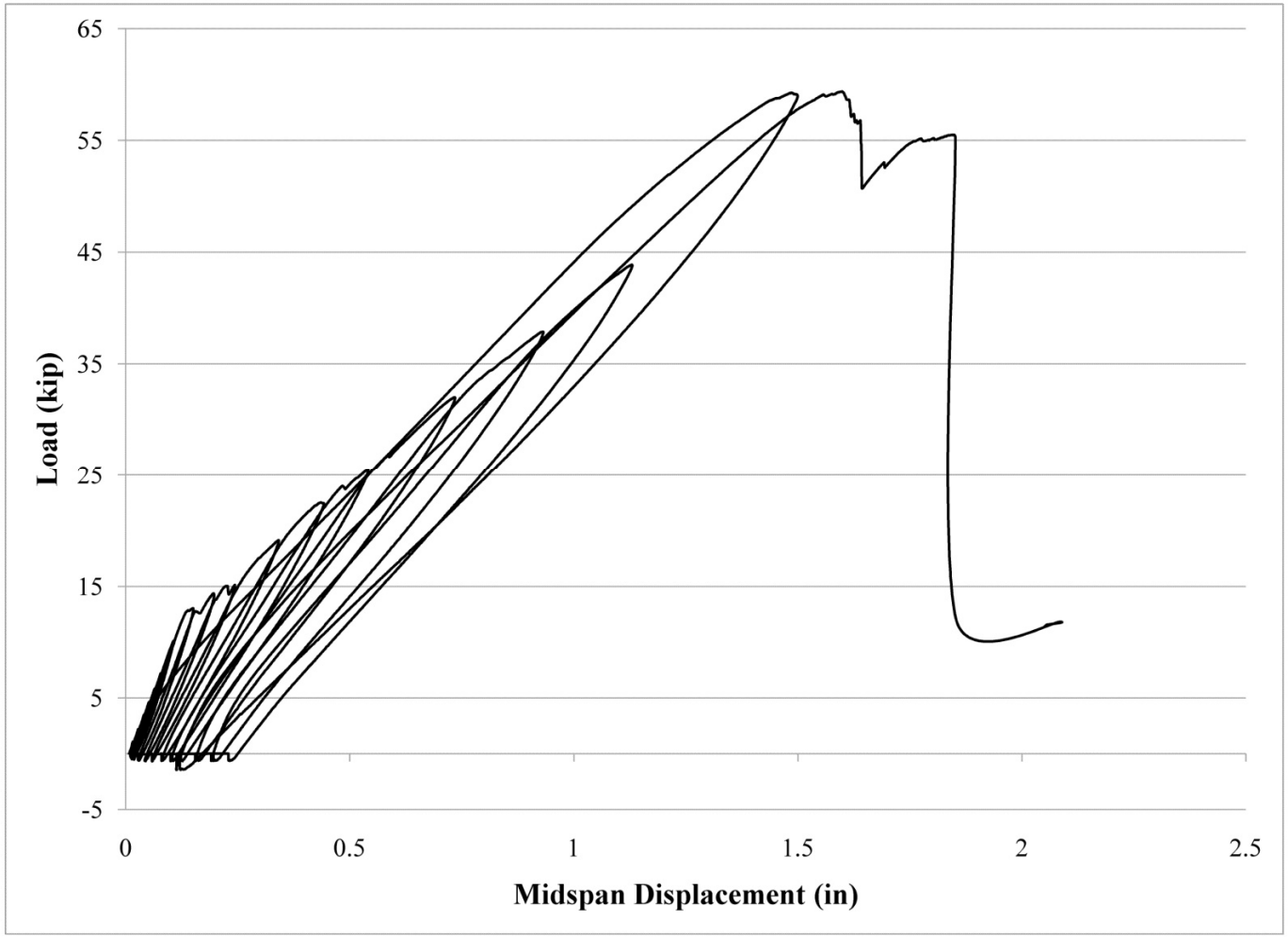

(b)

Figure 14 continued

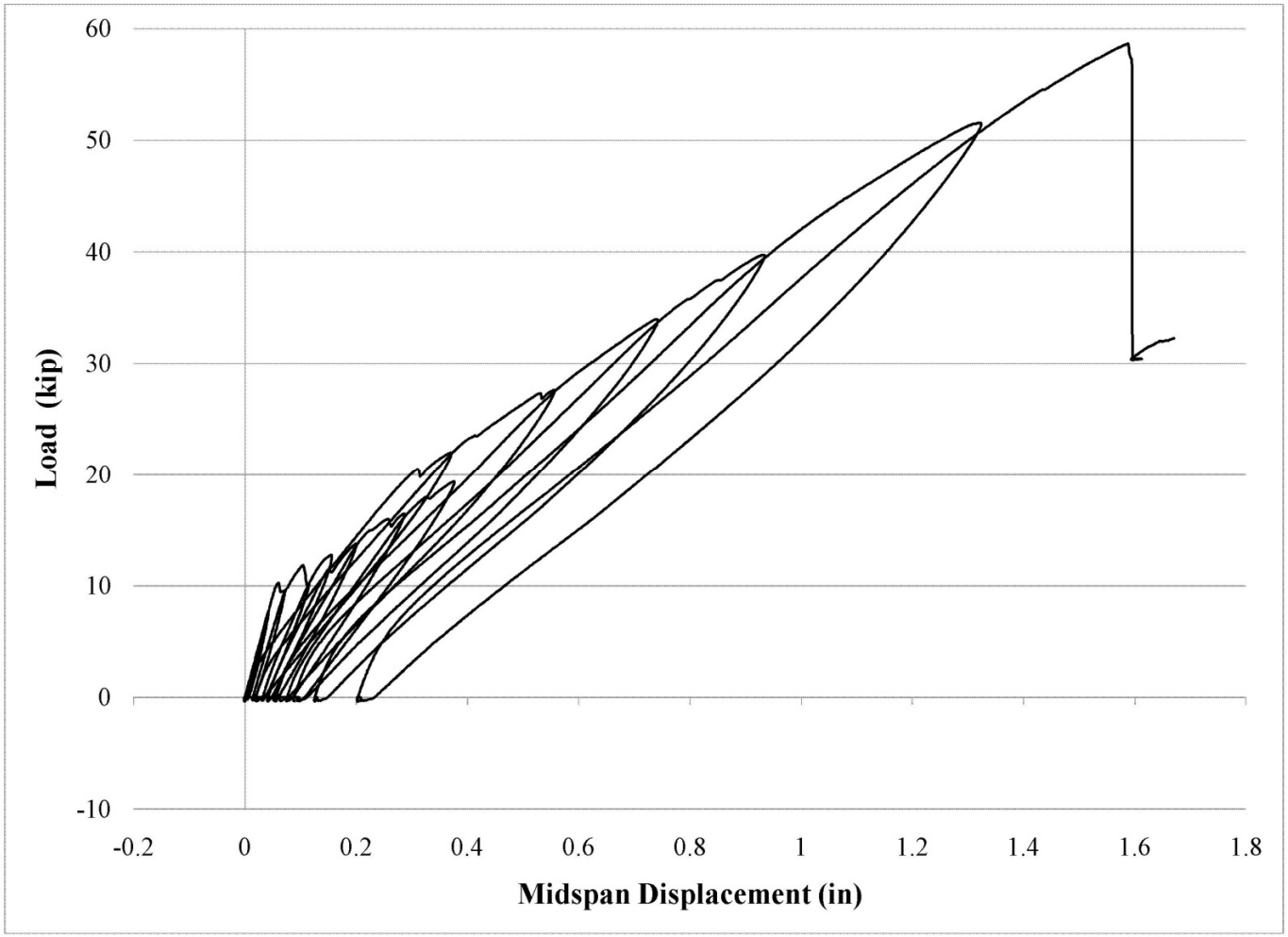

(c)
Figure 14 continued

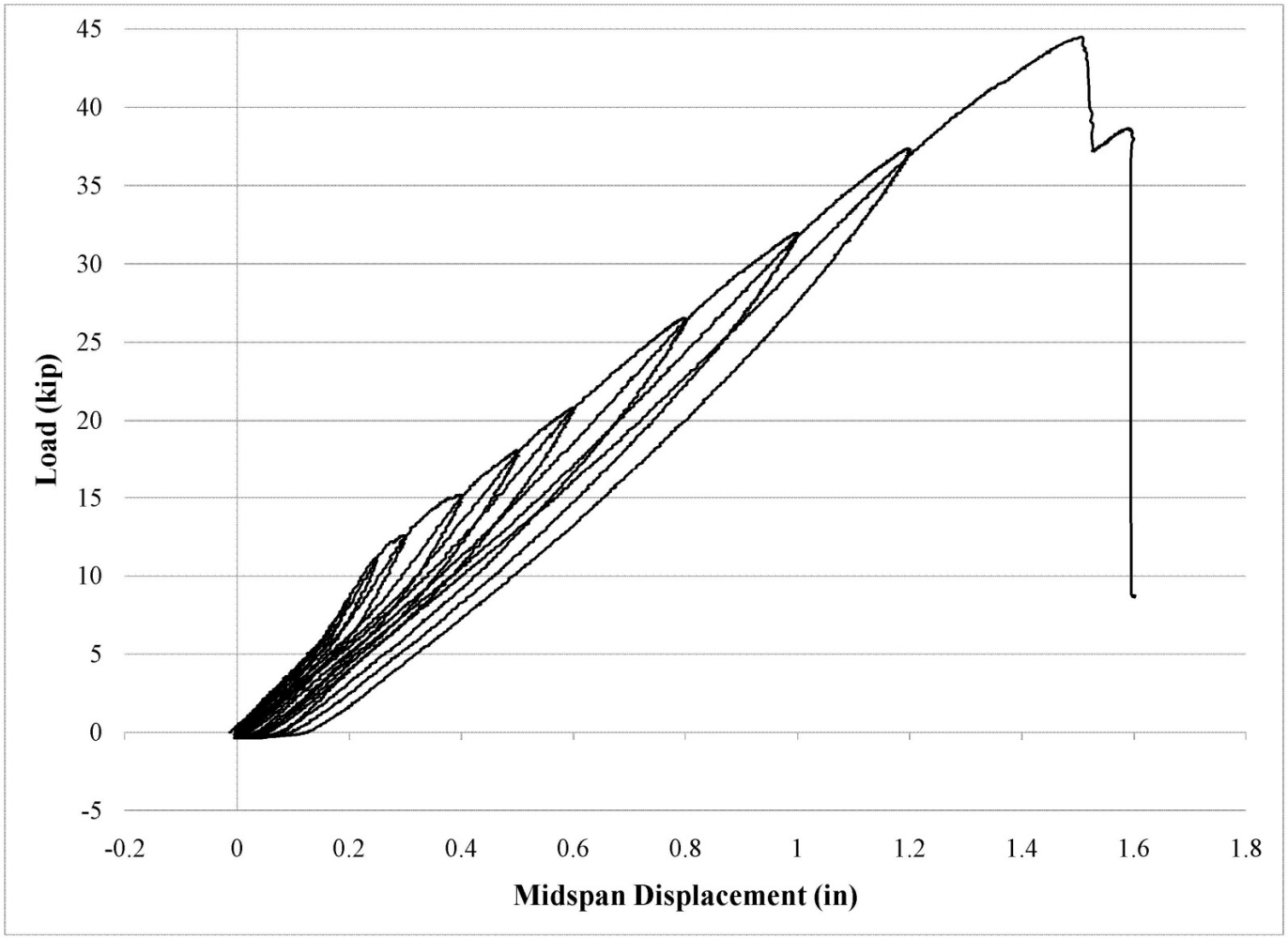

(d)
Figure 14 continued

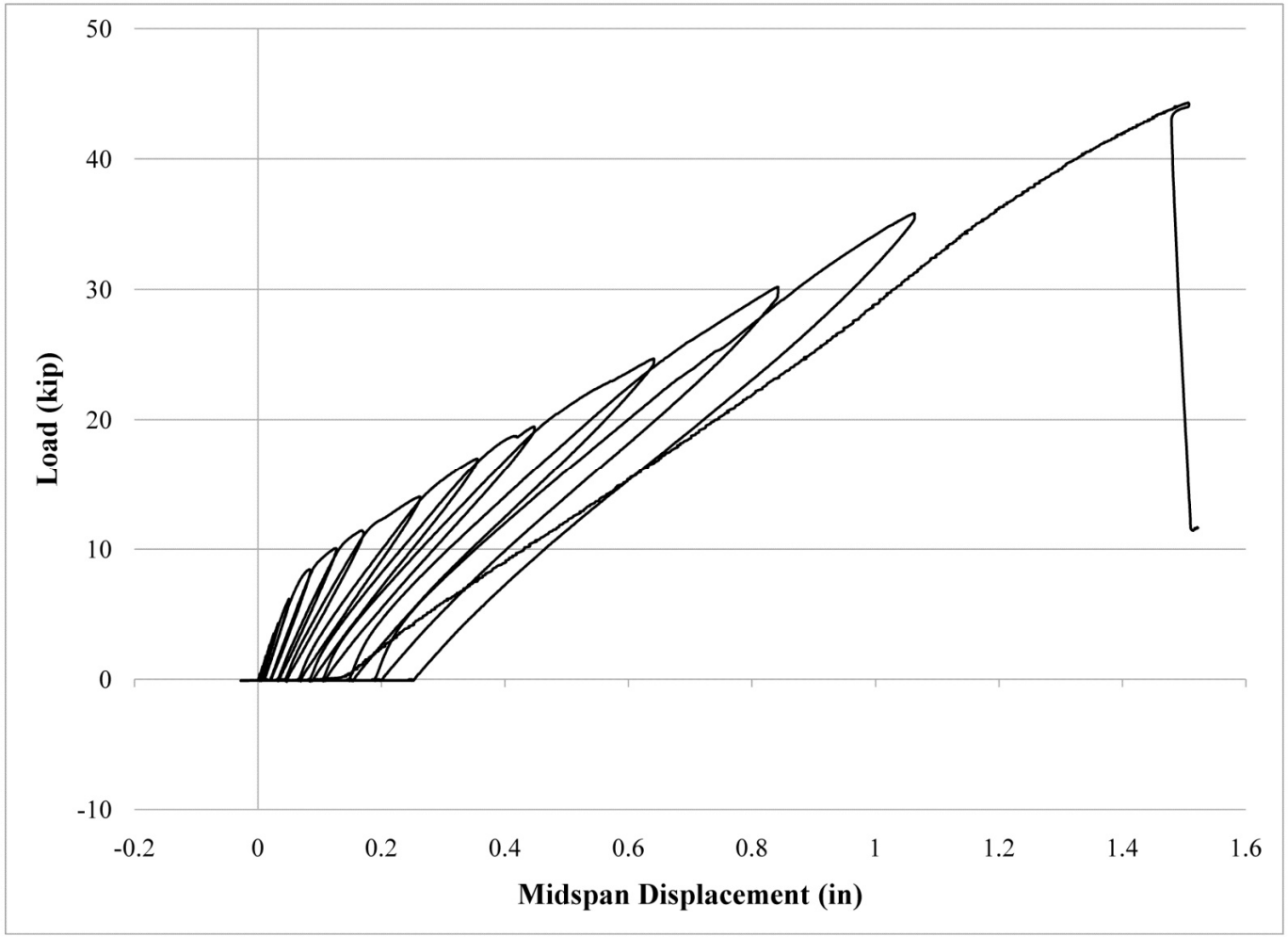

(e)
Figure 14 continued

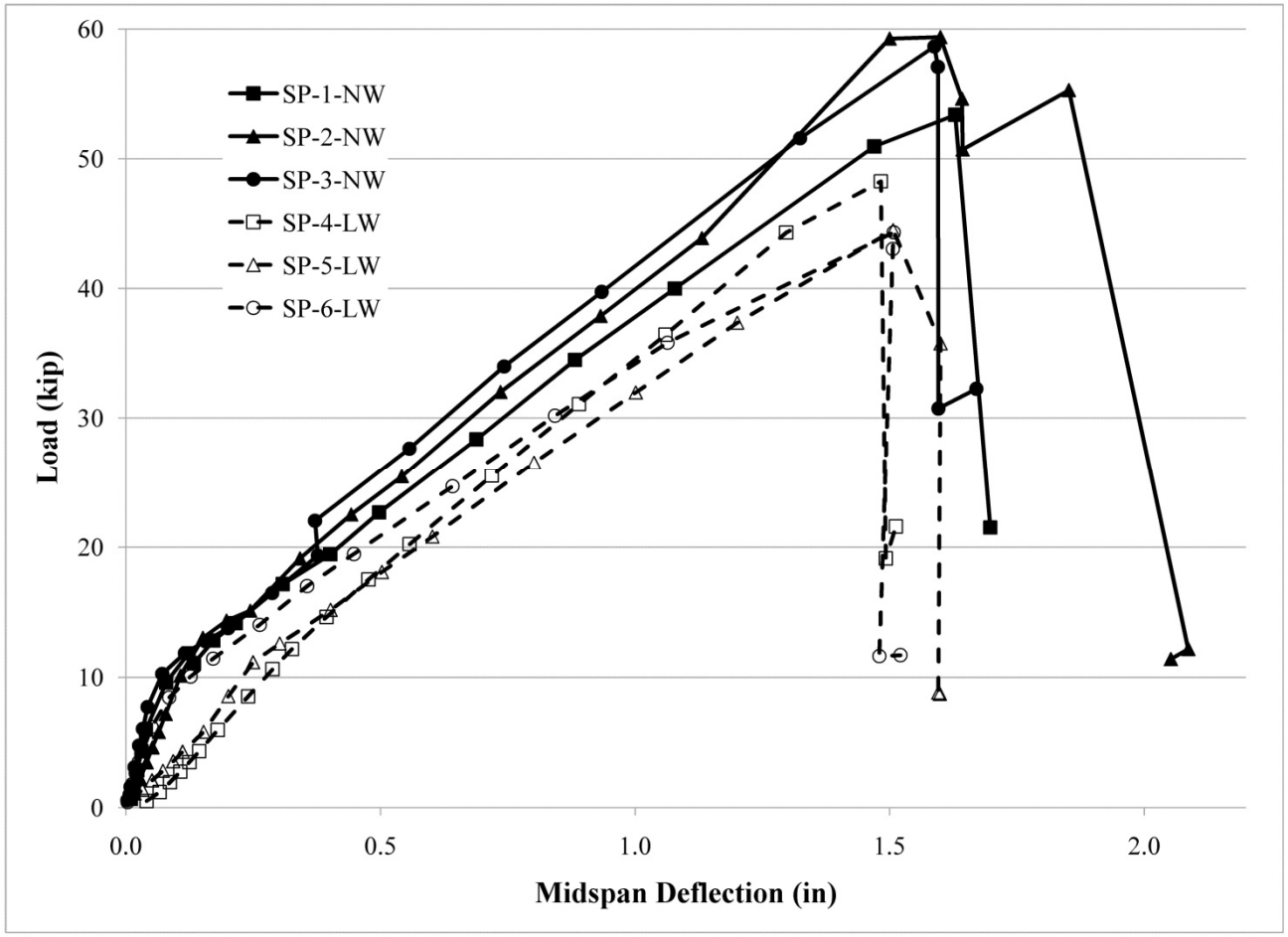

Figure 15 – Load-displacement envelopes of all specimens

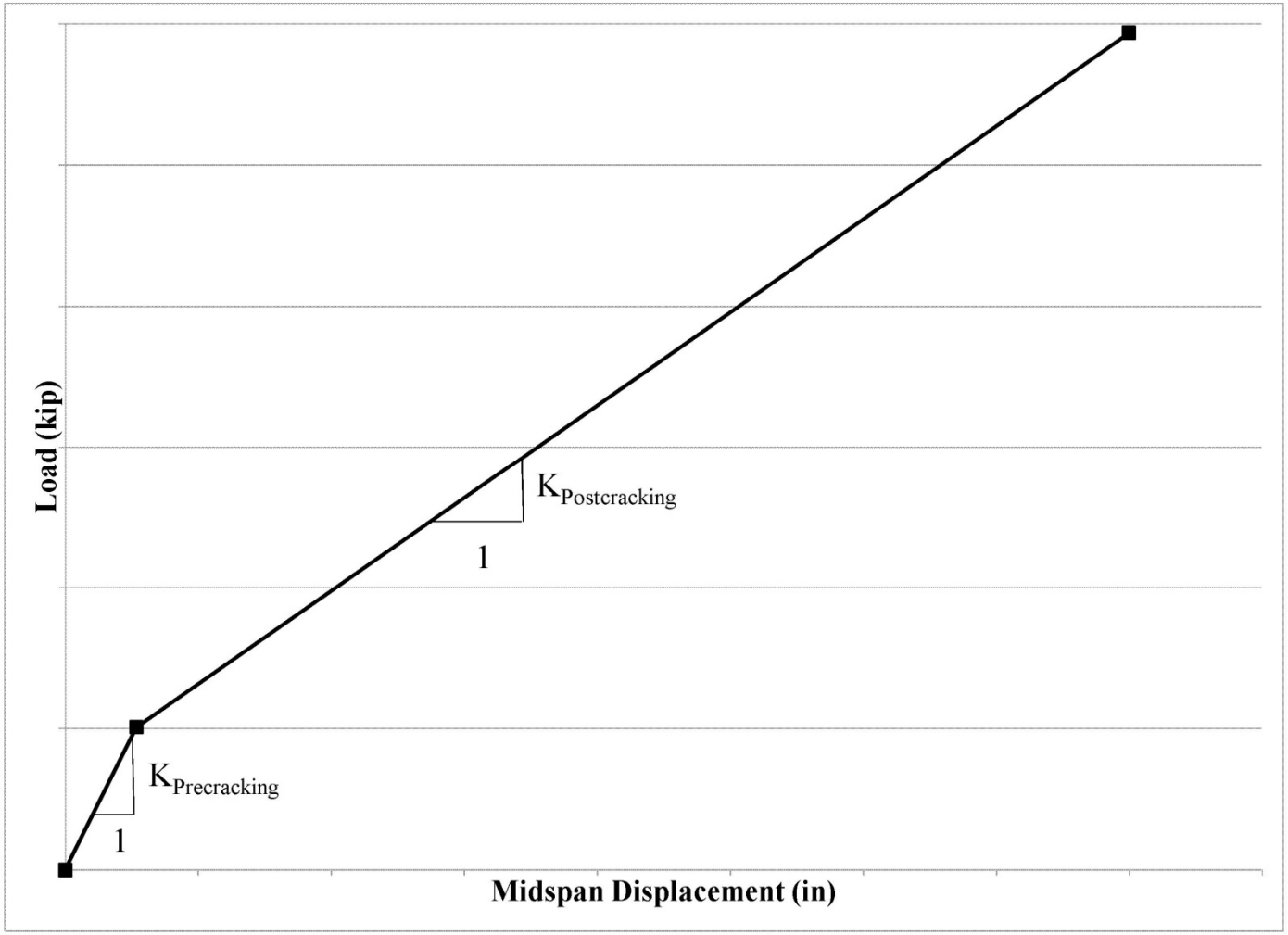

Figure 16 – Schematic of precracking and postcracking stiffness

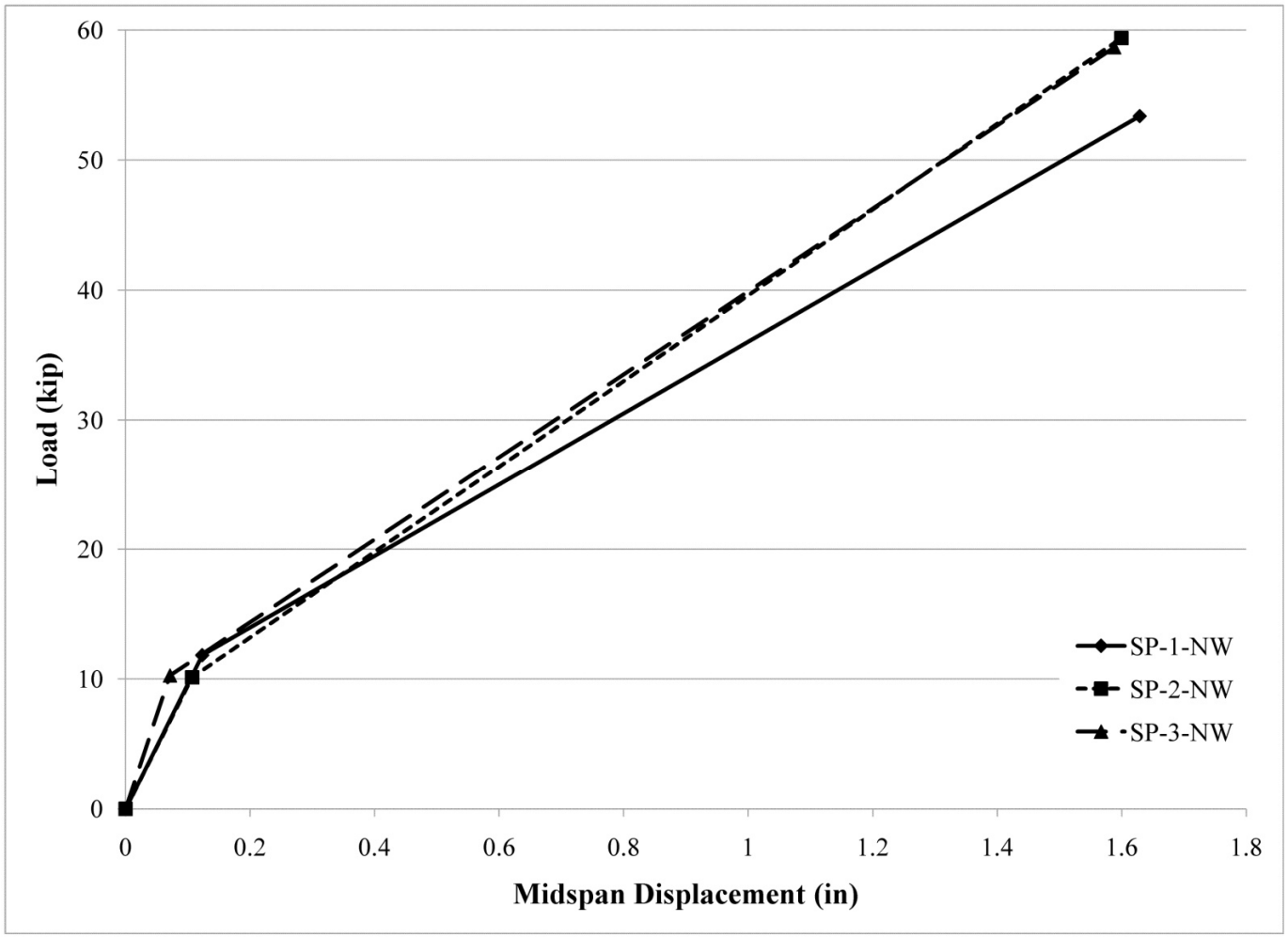

(a)

Figure 17 – Simplified stiffness of specimens: (a) Normal weight concrete specimens.
(b) Lightweight concrete specimens

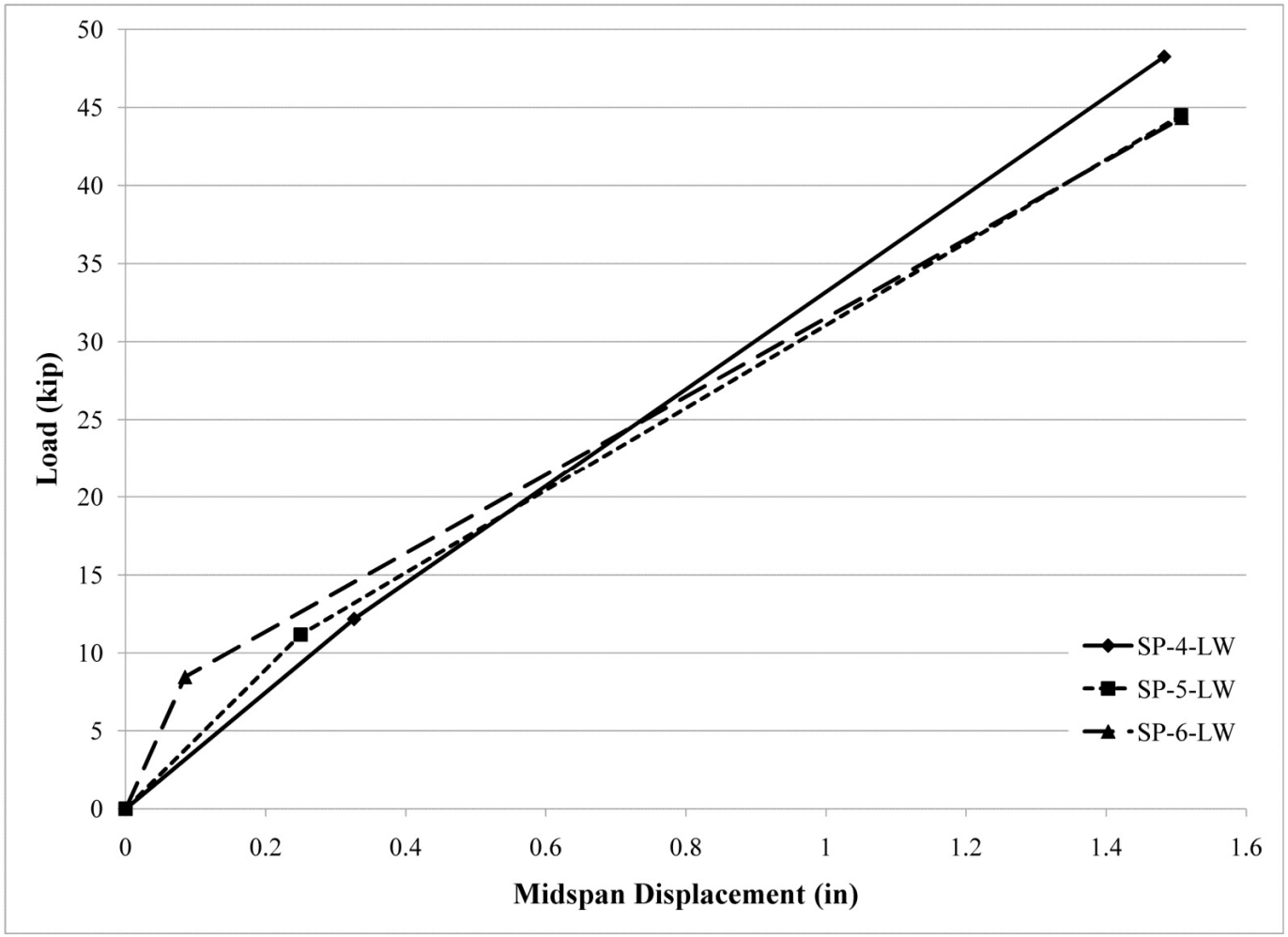

(b)
Figure 17 continued

Table 2 – Precracking stiffness and postcracking stiffness

Designation	Max Pre-cracking Load (kip)	Max Pre-cracking Displacement (in)	Max Post-cracking Load (kip)	Max Post-cracking Displacement (in)	Pre-cracking Stiffness (kip/in)	Post-cracking Stiffness (kip/in)	Postcracking/ Precracking (%)
SP-1-NW	11.84	0.12	53.38	1.63	96.3	27.6	29
SP-2-NW	10.13	0.11	59.37	1.60	94.7	33.0	35
SP-3-NW	10.27	0.07	58.65	1.59	144.2	31.9	22
SP-4-LW	12.18	0.33	48.25	1.48	37.3	31.2	84
SP-5-LW	11.17	0.25	44.50	1.51	44.7	26.5	59
SP-6-LW	8.45	0.08	44.32	1.51	99.7	25.2	25

Note - NW = Normal weight concrete
LW = Lightweight concrete

Table 3 – Strain (microstrain) in GFRP reinforcement at different service levels

Designation	L/800 = 0.12"	L/480 = 0.20"	L/180 = 0.53"	Ultimate	Percent of Ultimate Tensile Strain (%)
SP-1-NW	1360	2061	3969	11664	73
SP-2-NW	1507	2336	5247	12158	76
SP-3-NW	829	1328	4368	11432	71
SP-4-LW	NA	NA	NA	NA	NA
SP-5-LW	932	1667	3789	9051	56
SP-6-LW	1351	3216	6728	12021	75

Note - NW = Normal weight concrete
LW = Lightweight concrete

Table 4 – Strain (microstrain) in concrete at different service levels

Designation	L/800 = 0.12"	L/480 = 0.20"	L/180 = 0.53"	Ultimate	Percent of Ultimate Compressive Strain (%)
SP-1-NW	NA	NA	NA	NA	NA
SP-2-NW	-165	-506	-982	-1968	66
SP-3-NW	NA	NA	-1284	-2156	72
SP-4-LW	NA	NA	NA	NA	NA
SP-5-LW	-203	-358	-822	-1820	61
SP-6-LW	-327	-691	-1362	-2213	74

Note - NW = Normal weight concrete
LW = Lightweight concrete

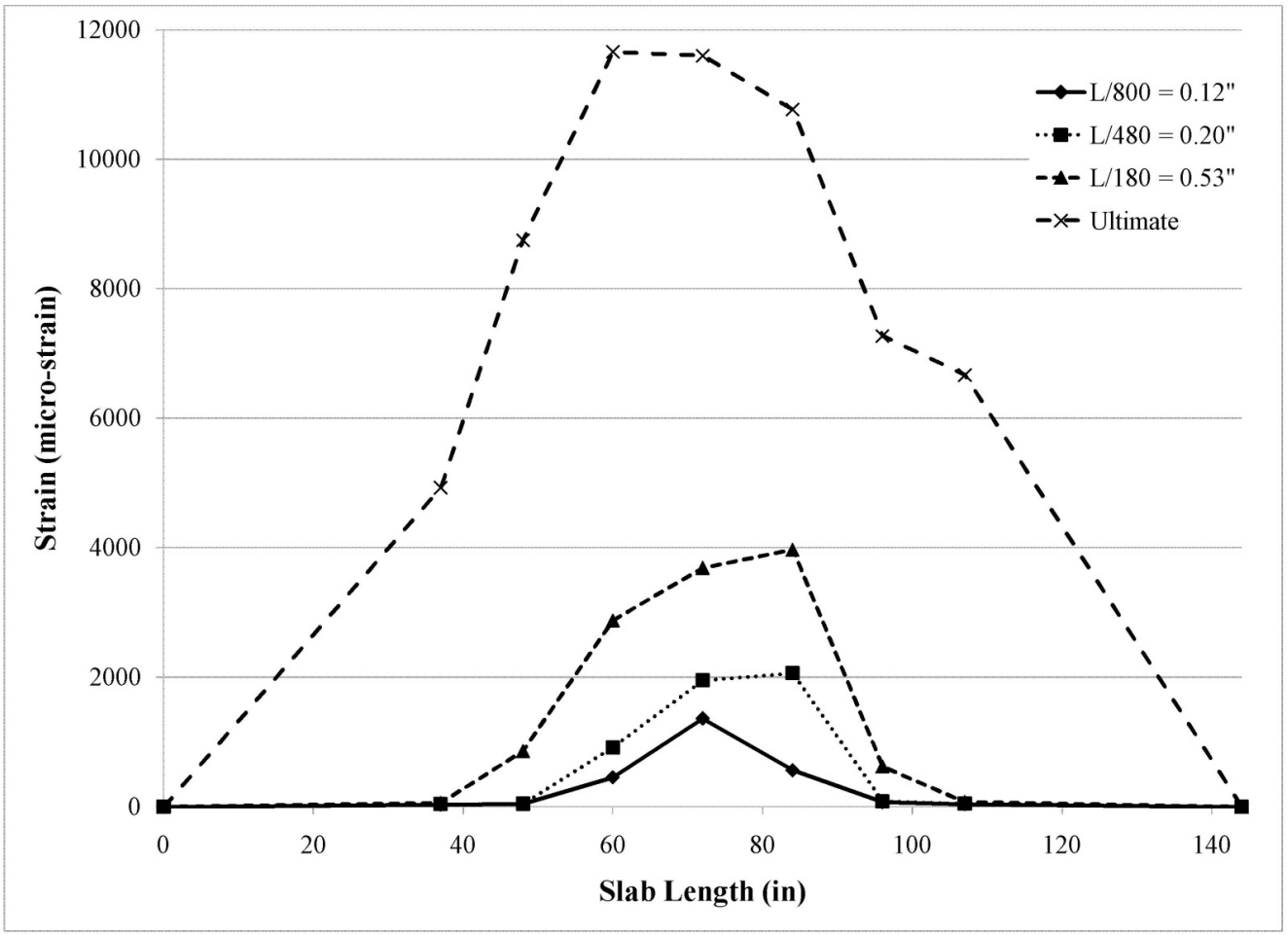

(a)

Figure 18 – Bottom reinforcement strain (microstrain) over slab length: (a) SP-1-NW strain over slab length, (b) SP-2-NW strain over slab length, (c) SP-3-NW strain over slab length, (d) SP-5-LW strain over slab length, (e) SP-6-LW strain over slab length

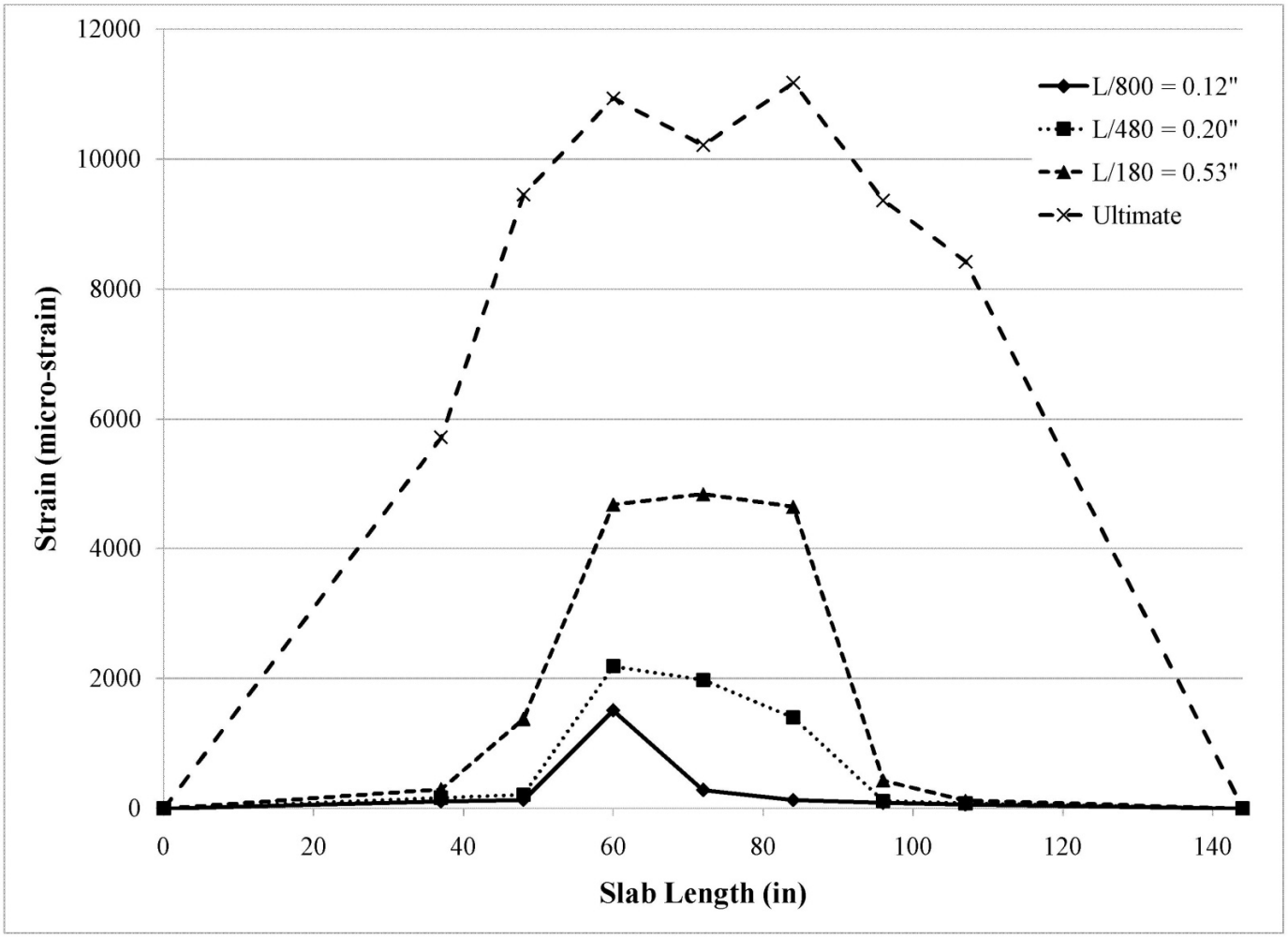

(b)
Figure 18 continued

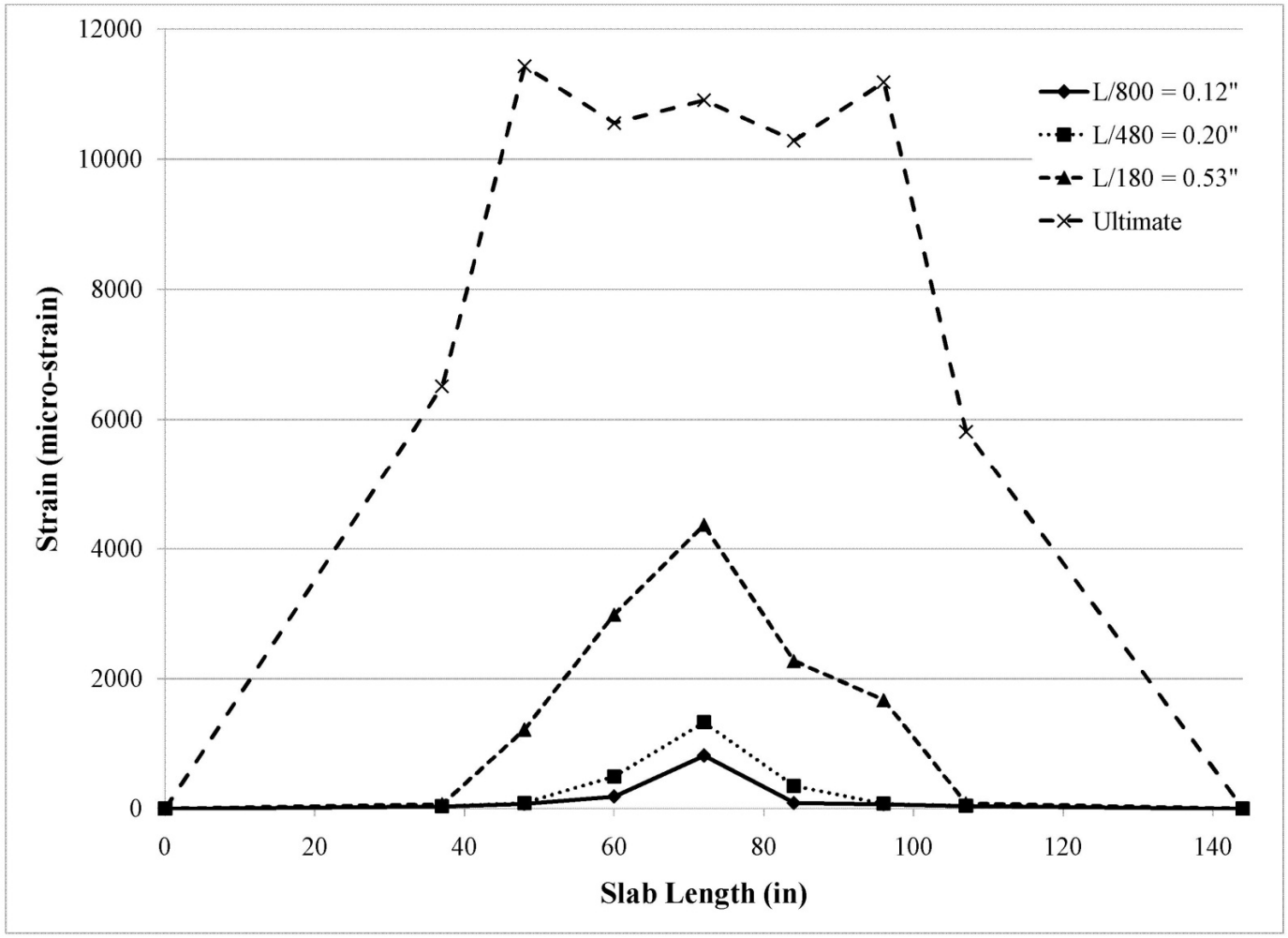

(c)
Figure 18 continued

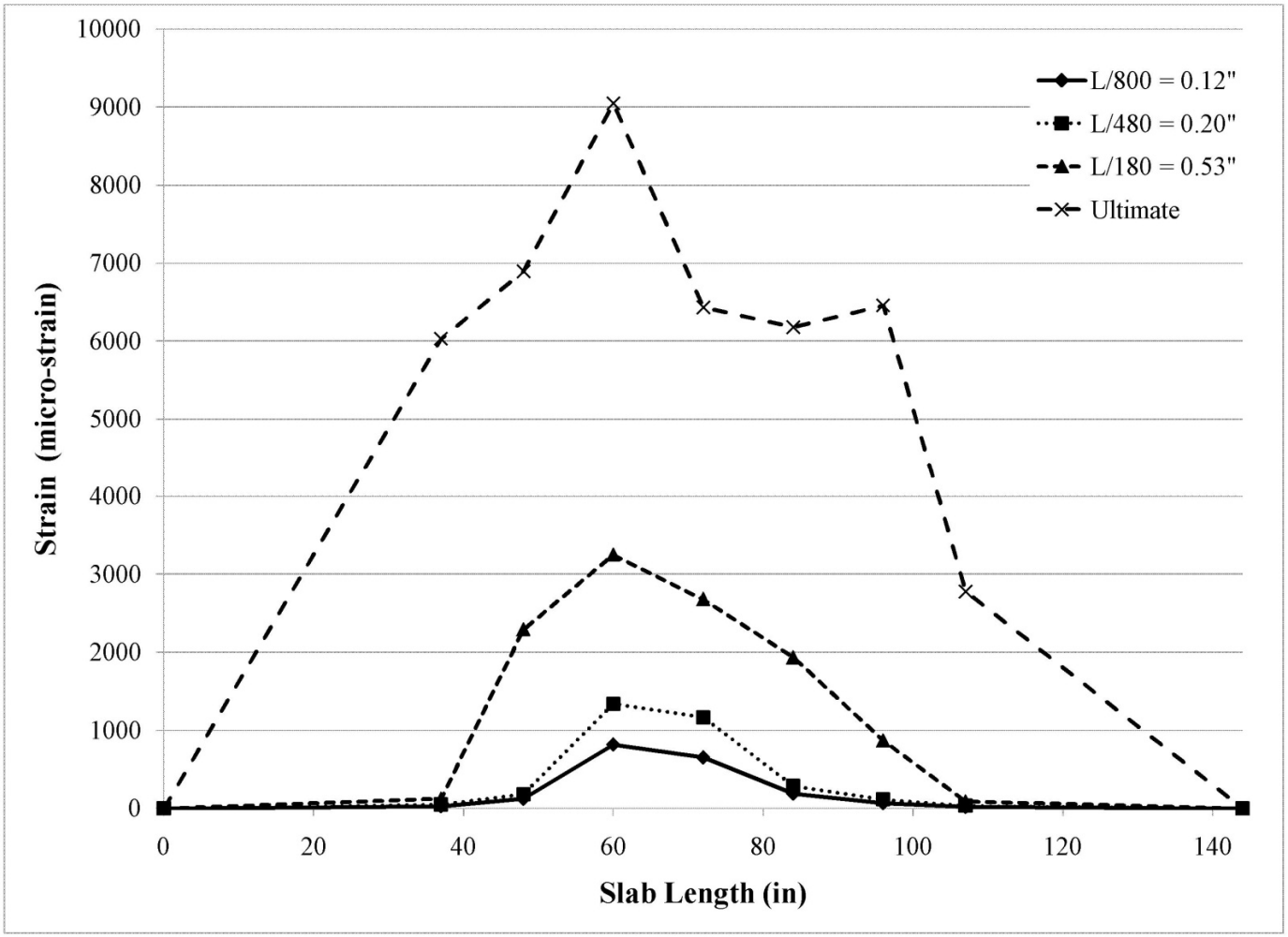

(d)

Figure 18 continued

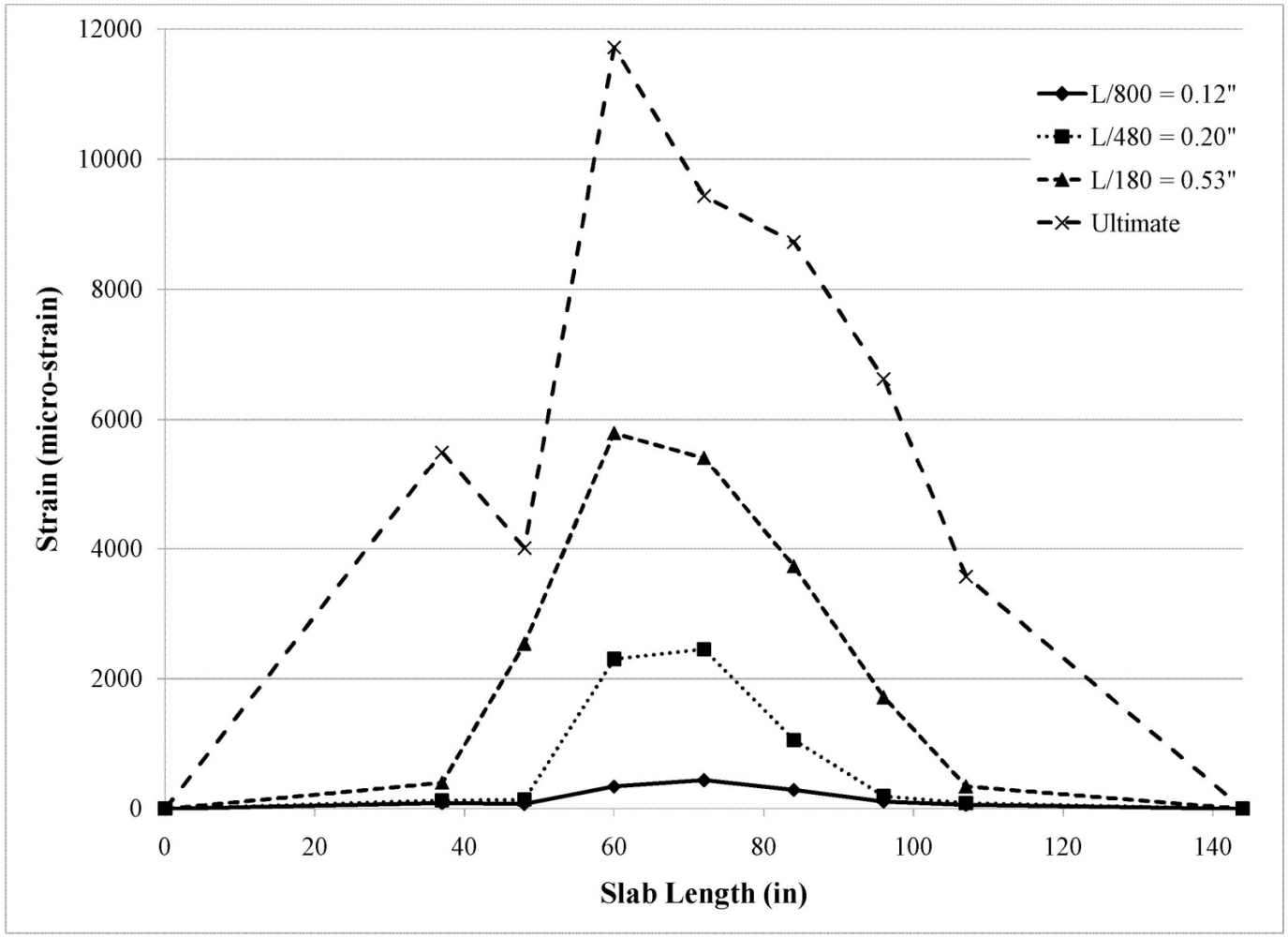

(e)
Figure 18 continued

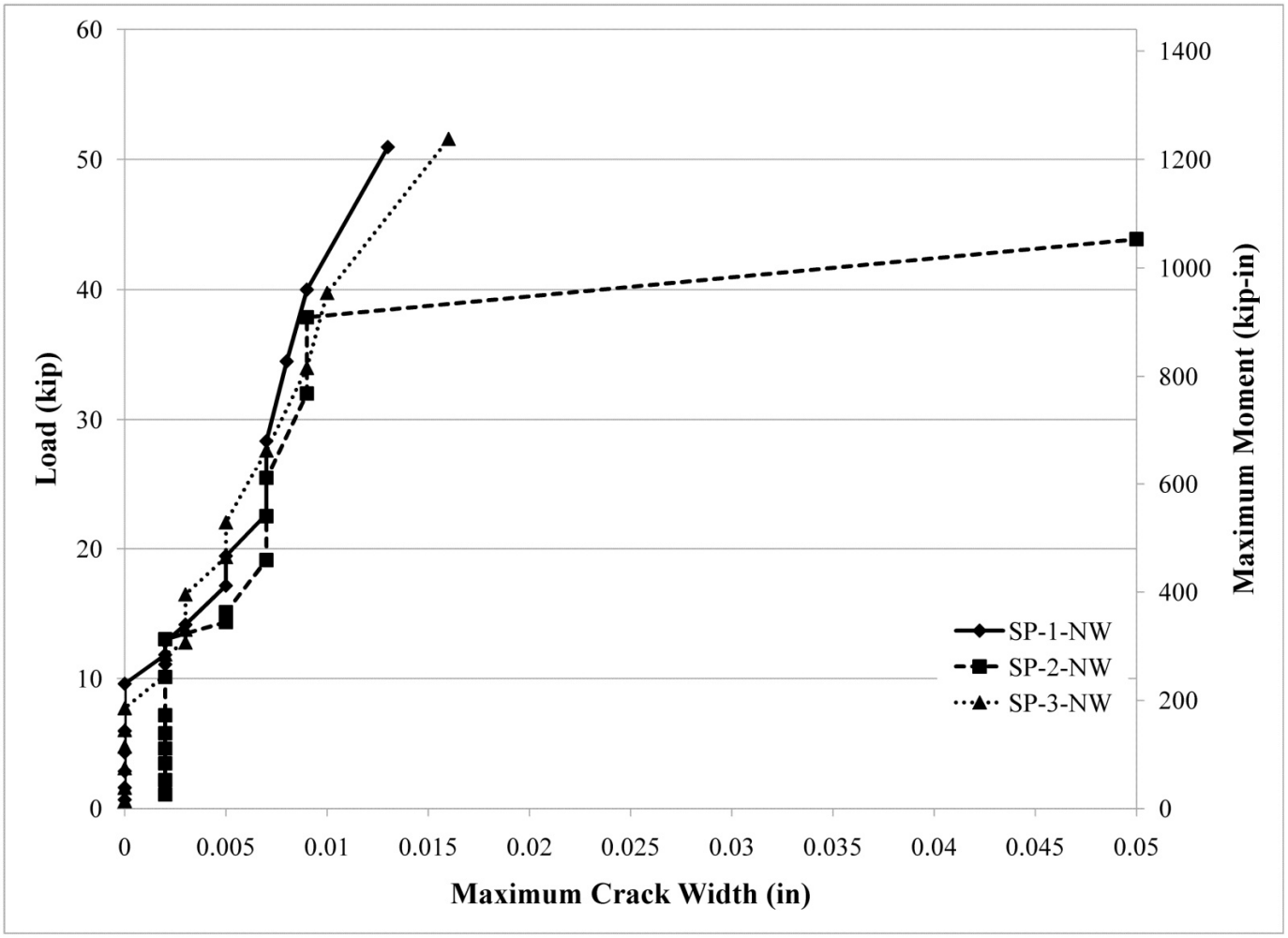

(a)

Figure 19 – Maximum crack width as load increases: (a) Normal weight concrete specimens, (b) Lightweight concrete specimens, (c) Detailed cracking all specimens

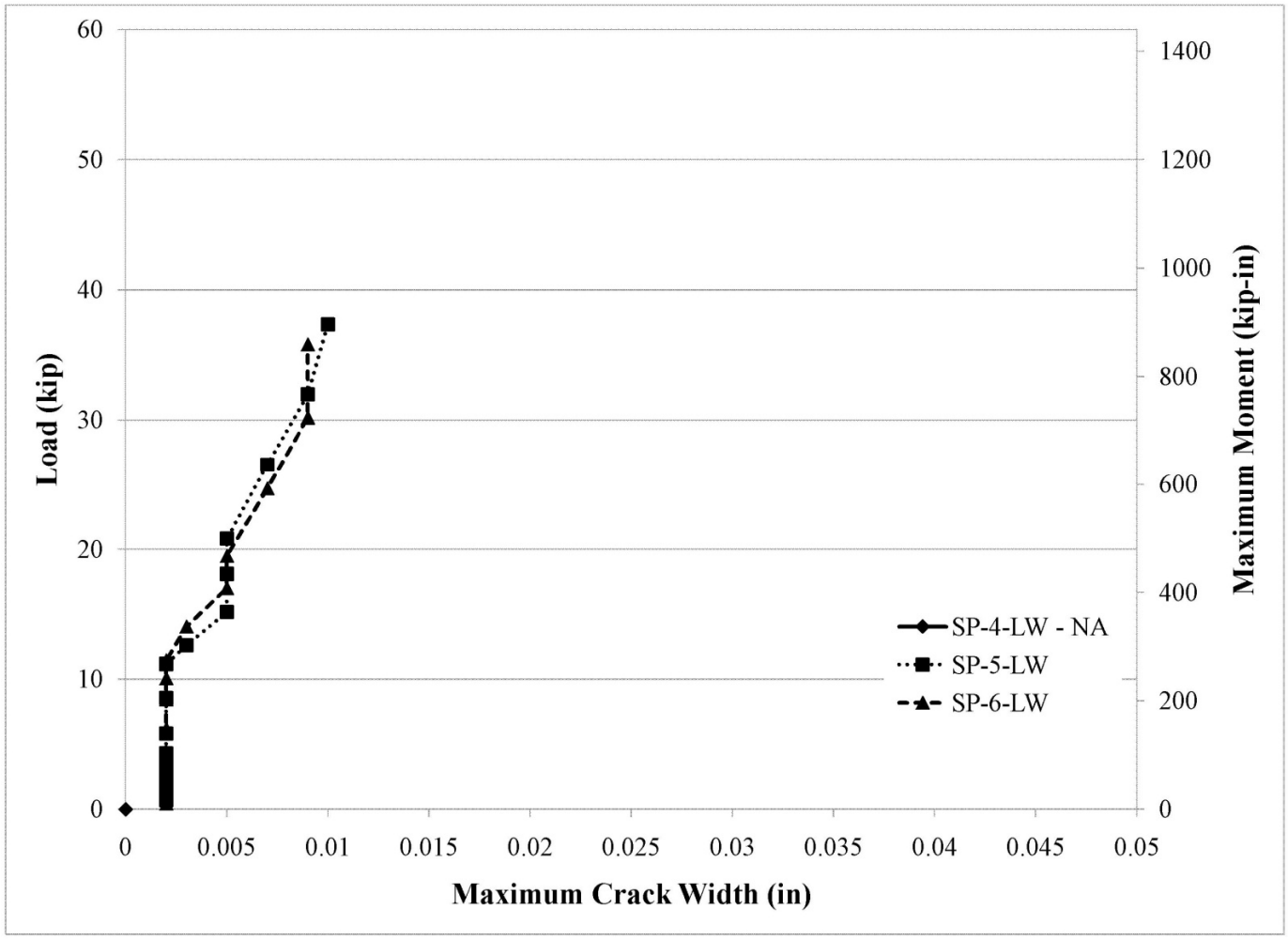

(b)

Figure 19 continued

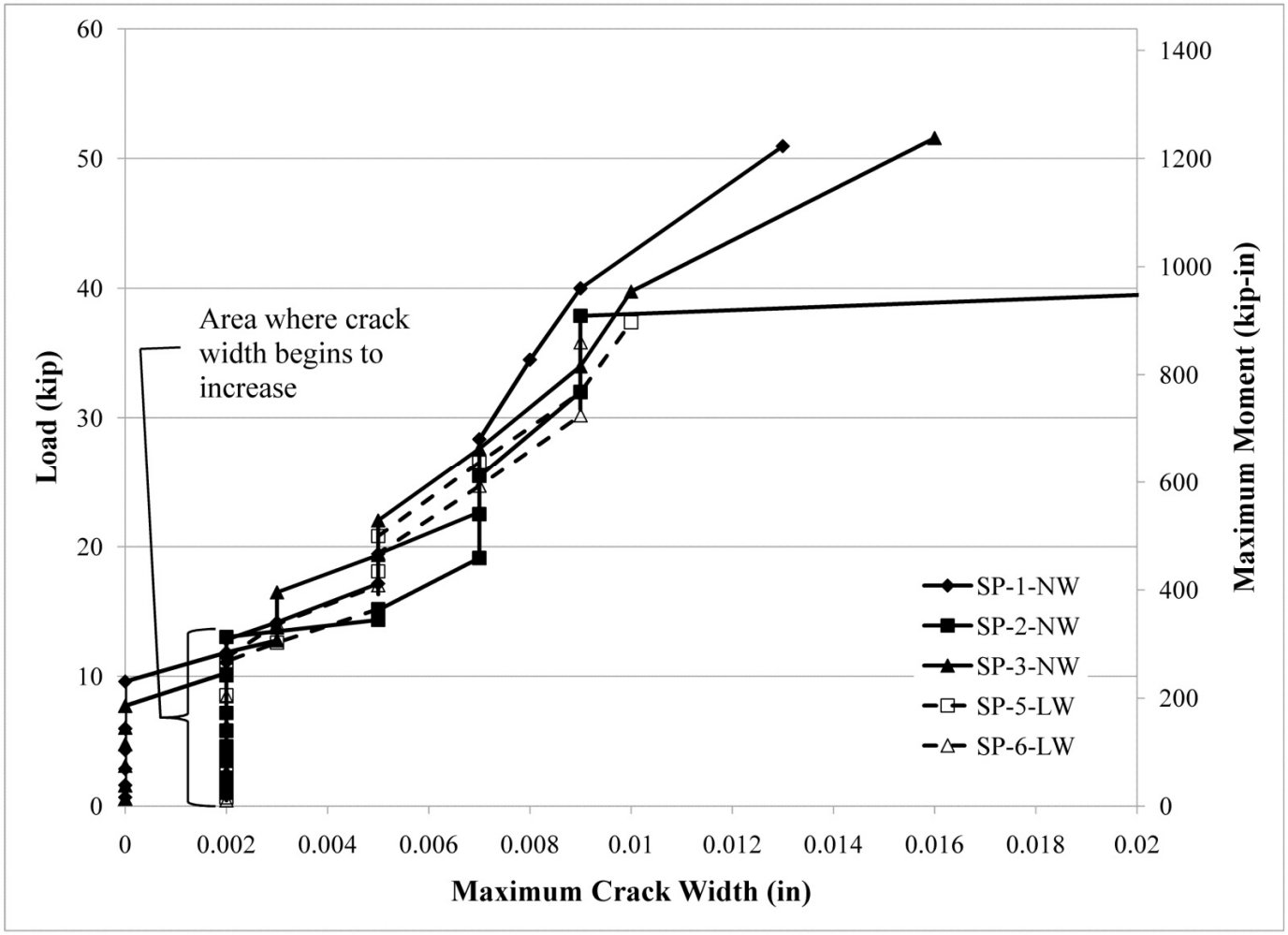

(c)
Figure 19 continued

Table 5 – Specimen cracking information. (a) SP-1-NW cracking information. (b) SP-2-NW cracking information. (c) SP-3-NW cracking information. (d) SP-5-LW cracking information. (e) SP-6-LW-D cracking information

(a)

Cycle	Load (kip)	Maximum Crack Width (in)	Number of Cracks	Average Crack Spacing (in)
1	0.69	0	0	0
2	1.61	0	0	0
3	2.87	0	0	0
4	4.33	0	0	0
5	5.98	0	0	0
6	9.61	0	0	0
7	11.84	0.002	1	0
8	11.10	0.002	2	6.00
8	12.83	0.002	3	6.50
9	14.16	0.003	3	6.50
10	17.16	0.005	7	6.50
11	19.45	0.005	10	4.60
12	22.67	0.007	10	4.60
13	28.35	0.007	12	5.36
14	34.48	0.008	12	5.36
15	39.99	0.009	16	4.26
16	50.94	0.013	20	3.24

Table 5 continued

(b)				
Cycle	**Load (kip)**	**Maximum Crack Width (in)**	**Number of Cracks**	**Average Crack Spacing (in)**
1	1.09	0.002	0	0
2	2.20	0.002	0	0
3	3.47	0.002	0	0
4	4.62	0.002	0	0
5	5.80	0.002	0	0
6	7.19	0.002	0	0
7	10.13	0.002	0	0
8	13.04	0.002	0	0
8	14.36	0.005	3	4.33
9	15.12	0.005	4	4.75
10	19.13	0.007	8	3.38
11	22.51	0.007	11	3.82
12	25.46	0.007	15	3.27
13	32.01	0.009	17	3.47
14	37.87	0.009	21	3.36
15	43.87	0.050	23	3.12

Table 5 continued

(c)				
Cycle	**Load (kip)**	**Maximum Crack Width (in)**	**Number of Cracks**	**Average Crack Spacing (in)**
1	0.57	0	0	0
2	1.60	0	0	0
3	3.11	0	0	0
4	4.77	0	0	0
5	6.05	0	0	0
6	7.73	0	0	0
7	10.27	0.002	1	0
8	11.86	0.002	2	7.00
8	12.78	0.003	3	7.00
9	13.78	0.003	4	6.00
10	16.48	0.003	6	5.00
11	19.36	0.005	7	5.15
12	22.03	0.005	8	5.31
13	27.63	0.007	10	5.40
14	33.98	0.009	11	4.90
15	39.73	0.010	14	4.78
16	51.57	0.016	22	3.18

Table 5 continued

(d)				
Cycle	**Load (kip)**	**Maximum Crack Width (in)**	**Number of Cracks**	**Average Crack Spacing (in)**
1	0.67	0.002	0	0
2	1.36	0.002	0	0
3	2.09	0.002	0	0
4	2.83	0.002	0	0
5	3.56	0.002	3	7.50
6	4.29	0.002	3	7.50
7	5.82	0.002	4	5.00
8	8.56	0.002	4	5.00
8	11.17	0.002	4	5.00
9	12.60	0.003	7	5.50
10	15.19	0.005	10	4.40
11	18.10	0.005	13	3.92
12	20.82	0.005	14	3.61
13	26.55	0.007	16	3.33
14	31.98	0.009	18	3.29
15	37.36	0.010	22	3.19

Table 5 continued

(e)				
Cycle	**Load (kip)**	**Maximum Crack Width (in)**	**Number of Cracks**	**Average Crack Spacing (in)**
1	0.44	0.002	0	0
2	1.01	0.002	0	0
3	1.83	0.002	0	0
4	2.65	0.002	0	0
5	3.51	0.002	0	0
6	4.33	0.002	0	0
7	6.19	0.002	0	0
8	8.45	0.002	0	0
8	10.07	0.002	3	6.50
9	11.44	0.002	4	4.50
10	14.04	0.003	8	3.85
11	17.01	0.005	10	4.55
12	19.48	0.005	12	4.36
13	24.70	0.007	15	4.25
14	30.19	0.009	17	3.69
15	35.82	0.009	21	3.10

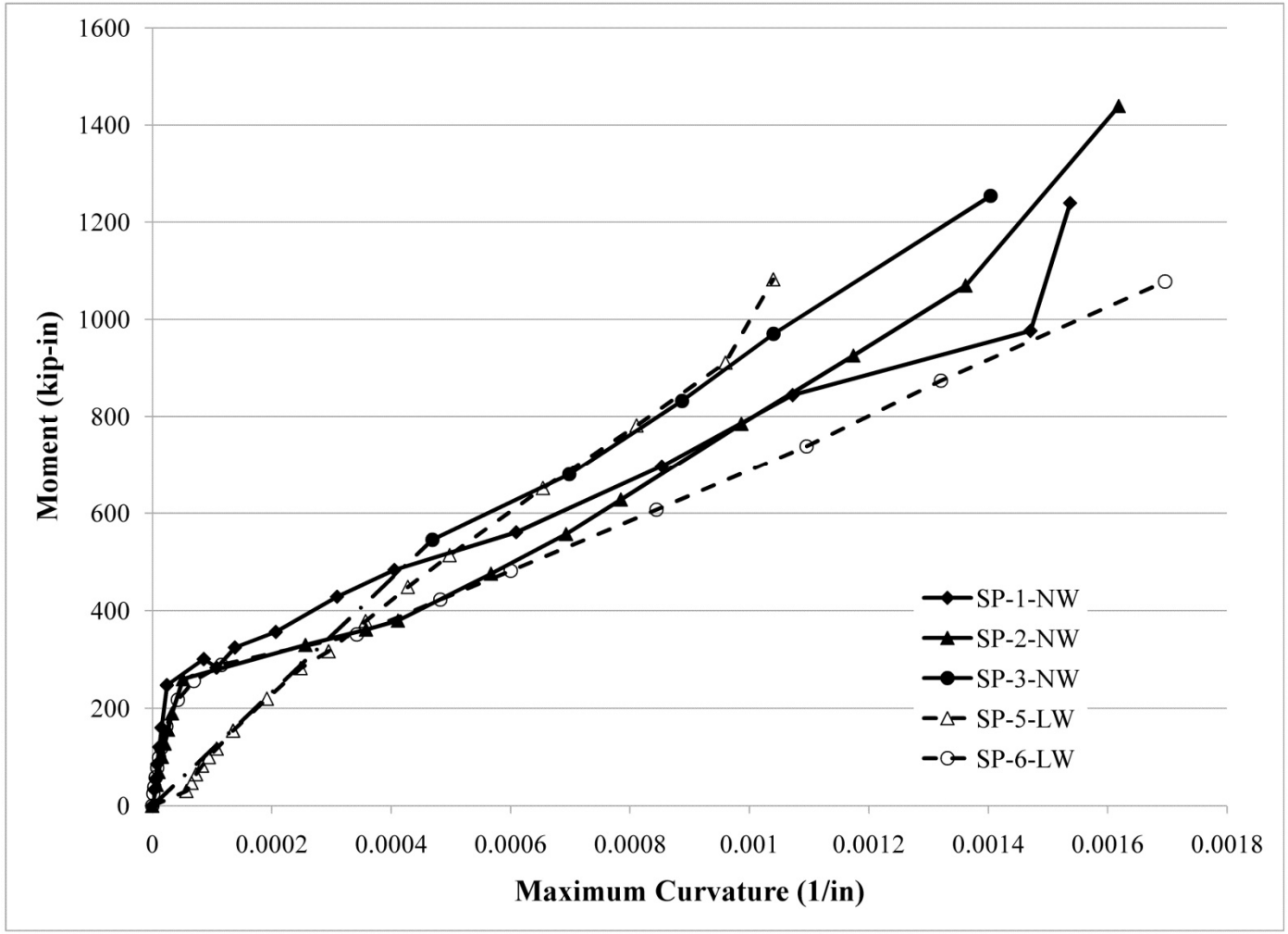

Figure 20 – Moment-curvature relationship for all specimens

Table 6 – Comparison of gross, uncracked and cracked moment of inertia

Designation	**I_g (in^4)**	**$I_{uncracked}$ (in^4)**	**$I_{cracked}$ (in^4)**	**$I_{uncracked}/I_g$ (%)**	**$I_{cracked}/I_g$ (%)**
SP-1-NW	1582.9	634.2	342.0	41	22
SP-6-LW	1582.9	932.8	447.2	59	29

Note - NW = Normal weight concrete
LW = Lightweight concrete

Table 7 – Summary of experimental results

Designation	f'c (psi)	Max Load (kip)	Actual Shear (kip)	ACI Predicted Shear (kip)	First-Order Predicted Shear* (kip)	Second-Order Predicted Shear** (kip)
SP-1-NW	8760	53.38	26.69	13.20	9.45	13.72
SP-2-NW	10370	59.37	29.69	13.93	9.89	14.45
SP-3-NW	12650	58.65	29.33	14.81	10.41	15.36
SP-4-LW	9090	48.66	24.33	14.89	8.64	12.33
SP-5-LW	8700	44.50	22.25	14.69	8.54	12.17
SP-6-LW	10930	44.32	22.16	15.79	9.07	13.06

Note - NW = Normal weight concrete
LW = Lightweight concrete
* = Houlte[3] first-order
** = Houlte[3] second-order

Table 8 – Comparison of actual shear to ACI predicted shear

Designation	f'c (psi)	Max Load (kip)	Actual Shear (kip)	ACI Predicted Shear (kip)	Actual Shear/ACI Predicted Shear
SP-1-NW	8760	53.38	26.69	13.20	2.02
SP-2-NW	10370	59.37	29.69	13.93	2.13
SP-3-NW	12650	58.65	29.33	14.81	1.98
SP-4-LW	9090	48.66	24.33	14.89	1.63
SP-5-LW	8700	44.50	22.25	14.69	1.51
SP-6-LW	10930	44.32	22.16	15.79	1.40

Note - NW = Normal weight concrete
LW = Lightweight concrete

Table 9 – Comparison of actual shear capacity to modified ACI shear prediction

Designation	f'c (psi)	Max Load (kip)	Actual Shear (kip)	Modified ACI Predicted Shear (kip)	Actual Shear/Modified ACI Predicted Shear
SP-1-NW	8760	53.38	26.69	13.20	2.02
SP-2-NW	10370	59.37	29.69	13.93	2.13
SP-3-NW	12650	58.65	29.33	14.81	1.98
SP-4-LW	9090	48.66	24.33	12.66	1.92
SP-5-LW	8700	44.50	22.25	12.48	1.78
SP-6-LW	10930	44.32	22.16	13.42	1.65

Note - NW = Normal weight concrete
LW = Lightweight concrete

Table 10 – Comparison of actual shear capacity to further modified ACI shear prediction

Designation	f'c (psi)	Max Load (kip)	Actual Shear (kip)	Modified ACI Predicted Shear (kip)	Actual Shear/Modified ACI Predicted Shear
SP-1-NW	8760	53.38	26.69	13.20	2.02
SP-2-NW	10370	59.37	29.69	13.93	2.13
SP-3-NW	12650	58.65	29.33	14.81	1.98
SP-4-LW	9090	48.66	24.33	11.17	2.18
SP-5-LW	8700	44.50	22.25	11.01	2.02
SP-6-LW	10930	44.32	22.16	11.84	1.87

Note - NW = Normal weight concrete
LW = Lightweight concrete

Table 11 – Comparison of actual shear capacity to Hoult first-order shear prediction

Designation	f'c (psi)	Max Load (kip)	Actual Shear (kip)	First-Order Predicted Shear* (kip)	Actual Shear/First-Order Shear*
SP-1-NW	8760	53.38	26.69	9.45	2.82
SP-2-NW	10370	59.37	29.69	9.89	3.00
SP-3-NW	12650	58.65	29.33	10.41	2.82
SP-4-LW	9090	48.66	24.33	8.64	2.82
SP-5-LW	8700	44.50	22.25	8.54	2.61
SP-6-LW	10930	44.32	22.16	9.07	2.44

Note - NW = Normal weight concrete
LW = Lightweight concrete
* = Hoult[3] first-order

Table 12 – Comparison of actual max strain, first-order predicted max strain and percent ultimate strain

Designation	Actual Max Strain (Microstrain)	Max Predicted Strain* (Microstrain)	Actual Strain/Predicted Strain*	Percent Ultimate Strain* (%)
SP-1-NW	11663	5721	2.04	36
SP-2-NW	12157	5982	2.03	37
SP-3-NW	11431	6302	1.81	39
SP-4-LW	NA	5225	NA	33
SP-5-LW	9050	5165	1.75	32
SP-6-LW	12020	5487	2.19	34

Note - NW = Normal weight concrete
LW = Lightweight concrete
* = Hoult[3] first-order

Table 13 - Comparison of actual shear capacity to Hoult second-order shear capacity

Designation	f'c (psi)	Max Load (kip)	Actual Shear (kip)	Second-Order Predicted Shear** (kip)	Actual Shear/Second-Order Shear**
SP-1-NW	8760	53.38	26.69	13.72	1.95
SP-2-NW	10370	59.37	29.69	14.45	2.05
SP-3-NW	12650	58.65	29.33	15.36	1.91
SP-4-LW	9090	48.66	24.33	12.33	1.97
SP-5-LW	8700	44.50	22.25	12.17	1.83
SP-6-LW	10930	44.32	22.16	13.06	1.70

Note - NW = Normal weight concrete
LW = Lightweight concrete
** = Hoult[3] second-order

Table 14 – Comparison of actual max strain, second-order predicted max strain and percent ultimate strain

Designation	Actual Max Strain (Microstrain)	Max Predicted Strain** (Microstrain)	Actual Strain/ Predicted Strain**	Percent Ultimate Strain** (%)
SP-1-NW	11663	8300	1.41	52
SP-2-NW	12158	8744	1.39	54
SP-3-NW	11431	9296	1.23	58
SP-4-LW	NA	7464	NA	47
SP-5-LW	9051	7363	1.23	46
SP-6-LW	12020	7904	1.52	49

Note - NW = Normal weight concrete
LW = Lightweight concrete
** = Hoult[3] second-order

CHAPTER 4

CONCLUSIONS AND RECOMMENDATIONS

The present research tested six specimens consisting of three lightweight concrete panels and three normal weight concrete panels reinforced with Glass Fiber Reinforced Polymer bars to determine the applicability of the current ACI shear provisions and shear capacity equations proposed by Hoult for the use of lightweight concrete reinforced with GFRP reinforcement. The specimens were sized and reinforced in a manner similar to precast bridge panels, with a clear span typical of prestressed concrete girders used in bridge construction. Failure of the normal weight concrete specimens as well as the lightweight concrete specimens was sudden, but not catastrophic. Failure consisted of an inclined shear crack propagating from one support to the point of loading and crushing of the concrete in the compression zone of the specimens. Rupture of the GFRP reinforcement did not occur in any of the normal weight concrete or lightweight concrete specimens.

All of the specimens were found to be able to support a load greater than the maximum AASHTO design truck. The normal weight concrete specimens were found to be able to support a higher load level and higher displacement level than the lightweight concrete specimens. The normal weight concrete specimens were also found to have a higher precracking stiffness than the lightweight concrete specimens, but the difference in the postcracking stiffness between the normal weight concrete specimens and the

lightweight concrete specimens was found to be smaller with a difference of 10% at the ultimate condition.

The strain level in the GFRP reinforcement of the normal weight concrete specimens and the lightweight concrete specimens was found to be similar during testing and at the ultimate condition, with an average difference of approximately 14% with neither concrete type showing consistently higher strain levels in the GFRP reinforcement. The strain in the concrete for the normal weight concrete specimens and the lightweight concrete specimens was also found to be at similar levels, with an average difference of approximately 11%, with neither concrete type showing consistently higher strain levels when the ultimate condition was reached and failure occurred.

It was found that the load level where the level of cracking changed the stiffness of the specimen from the precracked stiffness to the postcracking stiffness is similar for both the normal weight concrete specimens and the lightweight concrete specimens, and occurred at approximately 12 kip. The normal weight concrete specimens were found to be able to obtain a maximum crack width that is greater than the lightweight concrete specimens. However, the number of cracks as well as the average crack spacing was found to be very similar for both the normal weight concrete specimens and the lightweight concrete specimens, with the final number of cracks for all specimens having a range of 20 to 23 cracks with an average crack spacing ranging from 3.10 inches to 3.24 inches.

The uncracked moment of inertia of the lightweight concrete specimens was found to be greater than the normal weight concrete specimens at the transition from the precracking stiffness to the postcracking stiffness. Additionally, the cracked moment of

inertia was found to be higher for the lightweight concrete specimens than the normal weight concrete specimens.

While the ability to resist applied load was greater for the normal weight concrete specimens when compared to the lightweight concrete specimens, the level of curvature was not found to be consistently greater for either the normal weight concrete specimens or the lightweight concrete specimens.

The current ACI 440.1R-06 does not give theoretical design information for the use of lightweight concrete reinforced with GFRP reinforcement. The ACI shear provisions for normal weight concrete reinforced with GFRP reinforcement were used to predict the shear capacity of the normal weight concrete specimens as well as the lightweight concrete specimens.

The actual shear capacity of the normal weight concrete specimens was found to be greater than the lightweight concrete specimens. However, the ACI predicted shear capacity of the normal weight concrete specimens was found to be less than the ACI predicted shear capacity of the lightweight concrete specimens. Using the ACI shear capacity prediction provided a safety factor for the normal weight concrete of approximately 2.0 and a safety factor of approximately 1.5 for the lightweight concrete specimens. By applying the standard strength reduction factor of 0.85 for sand-lightweight concrete to the ACI shear prediction for normal weight concrete produces a safety factor of approximately 1.8 for the lightweight concrete specimens. Reducing the strength reduction factor from 0.85 to 0.75 provides a safety factor of approximately 2.0 for the lightweight concrete specimens. Due to the small number of tests conducted, it is recommended that additional research be done on lightweight concrete members of

various sizes and reinforcement ratios prior to the implementation of a strength reduction factor.

It was found that the first-order shear prediction proposed by Hoult provides a factor of safety for normal weight concrete specimens of approximately 2.8 and approximately 2.6 for the lightweight concrete specimens. The overly conservative shear prediction of the Hoult first-order shear prediction is the result of an underestimation of the strain in the longitudinal reinforcement. For the first-order shear prediction proposed by Hoult to be more efficient for both normal weight concrete and lightweight concrete reinforced with GFRP reinforcement, a modification factor allowing for a higher level of strain in the GFRP reinforcement should be adopted. Additional research must be conducted on normal weight concrete specimens and lightweight concrete specimens of varying size and reinforcement ratios to determine what an appropriate modification factor would be.

The second-order shear prediction proposed by Hoult provides a factor of safety of 2 and 1.8 for normal weight concrete and lightweight concrete, respectively. The second-order shear equation provides shear predictions which are less conservative than the first-order shear predictions but are still reasonable for both normal weight concrete and lightweight concrete reinforced with GFRP reinforcement. The second-order shear prediction is less conservative and more appropriate for GFRP reinforced concrete members because it takes advantage of the higher obtainable strain levels in the GFRP reinforcement prior to failure. It is believed that a strength reduction modification factor does not need to be applied to the second-order shear prediction for lightweight concrete reinforced with GFRP reinforcement, but additional research should be conducted on

lightweight concrete specimens of varying size and reinforcement ratios to verify that a strength reduction factor is not needed.

From the testing and analysis described previously, it can be seen that precast lightweight concrete panels reinforced with GFRP reinforcement have many beneficial properties and a predictable performance that can be used in design. Once the additional recommended research has been conducted, the use of precast lightweight concrete panels reinforced with GFRP reinforcement should be considered in areas where deterioration of steel reinforcement is an issue or where reinforcement needs to be thermally and electrically nonconductive, and precast concrete elements are used.

REFERENCES

1. ACI Committee 440, 2006, *Guide for the design and construction of structural concrete reinforced with FRP bars (ACI 440.1R-06)*, American Concrete Institute, Farmington Hills, MI.

2. American Association of State and Highway Transportation Officials, 2009, *AASHTO LRFD bridge design guide specifications for GFRP reinforced concrete bridge decks and traffic railings,* 1st Ed., American Association of State Highway Transportation Officials, Washington, DC.

3. Hoult, N.A., Sherwood, E.G., Bentz, E.C., Collins, M.P., 2008, "Does the use of FRP reinforcement change the one-way shear behavior of reinforced concrete slabs?," *Journal of Composites For Construction*, 12(2), 125-133.

4. Utelite Corporation, 2010, *What is Utelite lightweight aggregate?*, May 2010, http://www.utelite.com/about_us.html.

5. Bentz, E.C., Vecchio, F.J., Collins, M.P., 2006, "The simplified MCFT for calculating the shear strength of reinforced concrete elements," *ACI Structural Journal*, 103(4), 614-624.

6. ASTM Committee C09.16, 2004, *Standard test method for compressive strength of concrete cylinders cast in place in cylindrical molds (ASTM C873/C873M-04e1)*, ASTM International, West Conshohocken, PA.

7. Tonias, D.E., Zhao, J.J., 2007, *Bridge Engineering,* 2nd Ed., McGraw-Hill, New York, NY.

8. ACI Standard, 2005, *Building code requirements for structural concrete and commentary (ACI 318-05/ACI 318R-05)*, American Concrete Institute, Farmington Hills, MI.